

# NISQ-compatible quantum cryptography based on Parrondo dynamics in discrete-time quantum walks

Aditi Rath,<sup>1, 2, \*</sup> Dinesh Kumar Panda,<sup>1, 2, †</sup> and Colin Benjamin<sup>1, 2, ‡</sup>

<sup>1</sup>*School of Physical Sciences, National Institute of Science Education and Research, Bhubaneswar, Jatni 752050, India*

<sup>2</sup>*Homi Bhabha National Institute, Training School Complex, Anushaktinagar, Mumbai 400094, India*

Compatibility with noisy intermediate-scale quantum (NISQ) devices is crucial for the realistic implementation of quantum cryptographic protocols. We investigate a cryptographic scheme based on discrete-time quantum walks (DTQWs) on cyclic graphs that exploits Parrondo dynamics, wherein periodic evolution emerges from a deterministic sequence of individually chaotic coin operators. We construct an explicit quantum circuit realization tailored to NISQ architectures and analyze its performance through numerical simulations in Qiskit under both ideal and noisy conditions. Protocol performance is quantified using probability distributions, Hellinger fidelity, and total variation distance. To assess security at the circuit level, we model intercept–resend and man-in-the-middle attacks and evaluate the resulting quantum bit error rate. In the absence of adversarial intervention, the protocol enables reliable message recovery, whereas eavesdropping induces characteristic disturbances that disrupt the periodic reconstruction mechanism. We further examine hardware feasibility on contemporary NISQ processors, specifically *ibm\_torino*, incorporating qubit connectivity and state-transfer constraints into the circuit design. Our analysis demonstrates that communication between spatially separated logical modules increases circuit depth via SWAP operations, leading to cumulative noise effects. By exploring hybrid state-transfer strategies, we show that qubit selection and connectivity play a decisive role in determining fidelity and overall protocol performance, highlighting hardware-dependent trade-offs in NISQ implementations.

## I. INTRODUCTION

The BB84 quantum key distribution (QKD) protocol [1] marked the beginning of quantum cryptography research, which was greatly bolstered by the E91 entanglement-based protocol [2]. Together, these pioneering schemes established that the fundamental principles of quantum mechanics, such as the impossibility of perfect state cloning [3] and the disturbance caused by measurement, could be used to generate secret keys with information-theoretic security. Since then, the field of QKD has grown substantially, giving rise to a wide variety of protocols, including decoy-state QKD [4], measurement-device-independent QKD [5], and device-independent QKD [6], all of which aim to enhance practical security under realistic imperfections.

While most experimentally realized QKD schemes rely on photonic encodings transmitted through optical channels [7–9], there is growing interest in cryptographic primitives that can be implemented directly on gate-based quantum processors. In particular, compatibility with noisy intermediate-scale quantum (NISQ) devices is increasingly important for testing and validating quantum communication protocols at the circuit level [10]. Discrete-time quantum walks (DTQWs) provide a promising platform in this direction. A DTQW consists of repeated applications of a coin and a conditional shift operations, leading to coherent spreading and interference across position states [11–13]. Unlike

classical random walks, quantum walks exhibit strong interference effects and parameter-dependent dynamical behavior. On cyclic graphs, the nature of the dynamics is highly sensitive to the choice of coin parameters, certain operators generate periodic revivals of the initial state, while others produce chaotic evolution [14].

A remarkable phenomenon in discrete-time quantum walks (DTQWs) is the emergence of Parrondo’s paradox. While originally formulated in classical game theory [15–18], its quantum realization on cyclic graphs has recently been explored [19, 20]. Two unitary operators that individually generate chaotic dynamics can, when combined in a deterministic sequence, produce fully periodic evolution. This interplay between chaos and order offers a natural mechanism for encoding and recovering information. In a cryptographic setting, one may exploit this asymmetry by generating a public state through a chaotic walk, while reserving the specific Parrondo sequence that restores periodicity as private information [19]. The forward evolution spreads a quantum state into an interference-rich distribution, whereas the correct inverse sequence reconstructs the original configuration. Although quantum walk-based cryptographic ideas have been proposed previously [21–26], a systematic circuit-level validation under realistic noise models and adversarial conditions remains limited. In particular, it is important to assess how such protocols behave when implemented using gate-based quantum circuits subject to connectivity constraints, state-transfer overhead, and hardware-level noise.

In this work, we present a comprehensive verification of DTQW-based cryptographic protocols that leverage Parrondo’s paradox. Specifically, we design efficient DTQW circuits using QFT-diagonalized shift operators [20, 27],

\* [aditi.rath@niser.ac.in](mailto:aditi.rath@niser.ac.in)

† [dineshkumar.quantum@gmail.com](mailto:dineshkumar.quantum@gmail.com)

‡ [colin.nano@gmail.com](mailto:colin.nano@gmail.com)

generate public keys from chaotic walk dynamics, encode messages via position-space translation operators, and decrypt messages using the periodic inverse evolution enabled by the Parrondo sequence. To evaluate the usability of such protocols on quantum processors, we employ a module-based simulation framework that assigns separate qubit registers to Alice, Bob, and Eve within a single quantum circuit. Communication steps, which include public-key transfer, message encoding, and adversarial interception, are simulated using SWAP operations. Using both ideal and noise-model simulations in `qiskit_aer` [28], we demonstrate accurate message recovery via the Parrondo strategies, robustness of the protocol under realistic quantum noise, and security under intercept-resend and man-in-the-middle attacks [29], with Eve's intervention destroying the walk periodicity required for decryption. We further analyze the feasibility of implementing the protocol on present-day NISQ hardware, `ibm_torino` [36], by mapping logically separated communicating parties onto distant qubit modules and simulating state transfer through SWAP operations and hybrid SWAP-teleportation operations, we quantify the impact of connectivity constraints on circuit depth and fidelity. Our results show that protocol performance depends sensitively on qubit choice, transpilation strategy, and hardware topology.

The manuscript is organized as follows. Sec. II introduces discrete-time quantum walks on cyclic graphs and the emergence of Parrondo's paradox. In Sec. III, we present the Parrondo's paradox-based quantum cryptographic protocol and its gate-level circuit implementation. Sec. IV discusses the numerical results obtained under ideal and noisy simulations. The security of the protocol against intercept-and-resend and man-in-the-middle attacks is analyzed in Sec. V. Sec. VI provides a comparative discussion with standard quantum cryptographic protocols. The challenges associated with implementing the protocol on present-day NISQ hardware are addressed in Sec. VII and Sec. VIII concludes with a summary and outlook. We provide the quantum circuit realizations obtained via Qiskit in Appendix A. In addition to the circuit realizations in Qiskit, we present proof-of-principle simulations in Mathematica [30] in Appendix B, given the current limitations of NISQ hardware [31] for distributed implementations [32]. Appendix C details the NISQ hardware implementation, results, and practical limitations.

## II. PARRONDO'S PARADOX VIA DTQWS ON CYCLIC GRAPHS

A DTQW evolving on a  $K$ -cycle graph is described in the composite Hilbert space,  $H_C \otimes H_P$ , where  $H_P$  denotes the position space and  $H_C$  implies the coin space. The coin space  $H_C$  is spanned on the basis  $\{|l\rangle\}$  i.e.,  $\{|0\rangle, |1\rangle\}$  and the position space  $H_P$  is defined on the vertices of the cyclic graph,  $\{|x\rangle : x \in \{0, 1, 2, \dots, K-1\}\}$ . Let

the walker be initialized at the vertex  $|0\rangle$  and is in a superposition of the coin states, its initial state is,

$$|\Phi(0)\rangle = (\cos\left(\frac{\Theta}{2}\right)|0\rangle + e^{i\omega} \sin\left(\frac{\Theta}{2}\right)|1\rangle) \otimes |K=0\rangle, \quad (1)$$

with  $0 \leq \Theta \leq \pi$  and  $0 \leq \omega < 2\pi$ . The coin operator has the form,

$$C(s, \gamma, \delta) = \begin{pmatrix} \sqrt{s} & \sqrt{1-s}e^{i\gamma} \\ \sqrt{1-s}e^{i\delta} & -\sqrt{s}e^{i(\gamma+\delta)} \end{pmatrix}, \quad (2)$$

with  $0 \leq s \leq 1$  and  $0 \leq \gamma, \delta \leq \pi$ .

The walker moves in counter-clockwise (clockwise) direction by one vertex conditioned on the coin state  $|0\rangle$  ( $|1\rangle$ ). The shift operator takes the form

$$S_K = \sum_{l=0}^1 |l\rangle\langle l| \otimes |F_l\rangle, \quad (3)$$

where  $F_l = \sum_{x=0}^{K-1} |(x + 2l - 1) \bmod K\rangle\langle x|$  with  $F_0 (F_1)$  denotes decrement (increment) shift operator corresponding to the counter-clockwise (clockwise) movement of the walker. The unitary single time step evolution operator generating the quantum walk is,

$$W = S_K \cdot (C \otimes I_K), \quad (4)$$

where  $I_K$  is an  $K \times K$  identity operator in the position space and  $W$  is a  $2K \times 2K$  circulant matrix formulated as [14],

$$W(s, \gamma, \delta) = \text{CIRC}_N \left( \begin{bmatrix} 0 & 0 \\ 0 & 0 \end{bmatrix}_0, \begin{bmatrix} \sqrt{s} & \sqrt{1-s}e^{i\gamma} \\ 0 & 0 \end{bmatrix}_1, \dots, \begin{bmatrix} 0 & 0 \\ \sqrt{1-s}e^{i\delta} & -\sqrt{s}e^{i(\gamma+\delta)} \end{bmatrix}_{K-1} \right). \quad (5)$$

After  $t$  steps, the final state is given by  $|\Phi(t)\rangle = W^t |\Phi(0)\rangle$ . If, after  $t = T$  steps, i.e.,

$$|\Phi(t = T)\rangle = W^T |\Phi(0)\rangle = |\Phi(0)\rangle, \quad (6)$$

then the quantum walk is called ordered (periodic), with period  $T$ , implying that the walker evolves back to its initial state with probability 1. If  $\{|y_j\rangle\}$  are the eigenvectors of  $W$  and  $\alpha_j$  are the eigenvalues, the initial state  $|\Phi(0)\rangle$  can be written as  $|\Phi(0)\rangle = \sum_{i=1}^{2K} a_i |y_i\rangle$  where  $a_i$  is the amplitude of the  $i$ th eigen vector. After  $t$  time steps, we get,

$$W^t |\Phi(0)\rangle = \sum_{i=1}^{2K} a_i \alpha_i^t |y_i\rangle. \quad (7)$$

Substituting Eq. (7) in Eq. (6) gives,

$$W^T = I_{2K}, \text{ or } \alpha_i^T = 1, \forall i \in [1, 2K], \quad (8)$$

which defines the criterion for periodic evolution. If  $W$  satisfies Eq.(8), it yields a periodic quantum walk. The

coin operator  $C$  decides whether the quantum walk would be ordered or not. For any arbitrary  $K$ -cyclic graphs, Ref. [14] gives the coin parameters that generate periodic walks.

Periodic quantum walks can also be generated by deterministically combining two chaotic walks, called Parrondo's paradox [15, 19, 20]. Here, unitary operators that individually yield chaotic walks with coins, say,  $A$  and  $B$ , are combined in a sequence  $AABB\dots$  to generate a periodic walk for arbitrary cyclic graphs. The chaotic coins  $A = C(s = 0.998489, \gamma = 0, \delta = 0)$  and  $B = C(s = 0.119545, \gamma = 0, \delta = 0)$  when combined in a sequence,  $AABB\dots$  produce a periodic walk with period 20 for 4-cycle graphs. Similarly, coins  $A' = C(s = 0.264734, \gamma = 0, \delta = 0)$  and  $B' = C(s = 0.801571, \gamma = 0, \delta = 0)$  combined in the Parrondo sequence,  $A'A'B'B'\dots$  yield an ordered walk with period 20 in 3-cycle graphs. Motivated by this interplay between order and chaos, we now develop a quantum cryptographic protocol in which periodicity emerging from chaotic operators enables a secure encryption-decryption mechanism.

### III. PARRONDO'S PARADOX-BASED QUANTUM CRYPTOGRAPHIC PROTOCOLS

#### A. Algorithm

Periodic walks on cyclic graphs generated via DTQW can be exploited to design a quantum cryptographic protocol [25]. The protocol uses the public key generation scheme for a secure encryption-decryption mechanism based on Parrondo's Paradox. Herein, we provide the steps required to execute a secure encryption-decryption of a message on arbitrary cyclic graphs.

**1. Generating a chaotic public key.** If Bob intends to send a message  $k \in \{0, 1, 2, \dots, K-1\}$  to Alice, where  $k$  is the vertex of the  $K$ -cyclic graph, then Alice first generates a public key based on the chaotic unitary operator  $W$  and the initial state of the walker  $|l\rangle|x\rangle$  as,

$$|\Phi_{PK}\rangle = W^t |l\rangle|x\rangle, \quad (9)$$

where  $W$  is the time evolution unitary operator that yields chaotic quantum walks on an  $K$ -cycle graph, and  $|x\rangle$  is the initial position state, while  $|l\rangle$  is the initial coin state of the walker. Alice sends the public key,  $|\Phi_{PK}\rangle$ , to Bob.

**2. Message Encryption.** Bob encodes the message  $k$  via,

$$|\Phi(k)\rangle = (I \otimes T_k) |\Phi_{PK}\rangle, \quad (10)$$

where  $I$  is the identity operator defined in the coin space and  $T_k = \sum_{i=0}^{K-1} |(i+k) \bmod K\rangle\langle i|$  similar to the shift operator described in Eq. (2) which acts only on the position state,  $|x\rangle$  thus,

$$T_k |x\rangle = |(k+x) \bmod K\rangle. \quad (11)$$

**3. Message Decryption.** Alice now decrypts the message by applying the Parrondo sequence  $G = W^{T-t}$  on  $|\Phi(k)\rangle$  with  $GW^t = W^T = I$ . Here, it is essential that  $[W, T_k] = 0$  [25], such that the periodicity condition emerging out of the Parrondo sequence can be satisfied. Further, Alice performs a measurement,  $M = \sum_{i=0}^{K-1} I \otimes |i\rangle\langle i|$  and receives the message  $k'$ . The original message can be recovered via

$$k = (k' - x) \bmod K. \quad (12)$$

#### B. Quantum Circuit realization

To realize the cryptographic protocol on the current generation quantum hardware (NISQ devices), we propose a quantum circuit following the approach in Ref. [20] for realizing quantum circuits for DTQW on cycles. Herein, we briefly outline the procedure to realize the DTQW on an even ( $K = 2^n$ ) cyclic graph on a quantum circuit. In a gate-based quantum circuit implementation, an  $K$ -cyclic graph is encoded using qubits. For an  $K = 2^n$  cyclic graph, the position Hilbert space is represented using  $n$  qubits, while a single additional qubit encodes the 2D coin space, thus requiring a total of  $n + 1$  qubits.

We illustrate the circuit construction using a 4-cycle graph. The shift operator is,

$$S_K = \begin{pmatrix} F_0 & \mathbf{0} \\ \mathbf{0} & F_1 \end{pmatrix}, \quad (13)$$

where  $\mathbf{0}$ 's represent  $K \times K$  null matrices in position space,  $F_0$  and  $F_1$  are the corresponding decrement and increment operators given as,

$$F_0 = \begin{pmatrix} 0 & 1 & 0 & 0 \\ 0 & 0 & 1 & 0 \\ 0 & 0 & 0 & 1 \\ 1 & 0 & 0 & 0 \end{pmatrix}, \text{ and } F_1 = \begin{pmatrix} 0 & 0 & 0 & 1 \\ 1 & 0 & 0 & 0 \\ 0 & 1 & 0 & 0 \\ 0 & 0 & 1 & 0 \end{pmatrix}. \quad (14)$$

To have an efficient circuit implementation, the shift operators are diagonalized via the quantum Fourier transform (QFT),  $M$  and  $M^\dagger$  given by,

$$F_0 = M^\dagger \mathcal{R}^\dagger M \text{ and } F_1 = M^\dagger \mathcal{R} M, \quad (15)$$

where  $\mathcal{R}(\mathcal{R}^\dagger)$  are the diagonalized shift (decrement and increment) operators with,

$$M = \frac{1}{2} \begin{pmatrix} 1 & 1 & 1 & 1 \\ 1 & r & r^2 & r^3 \\ 1 & r^2 & r^4 & r^6 \\ 1 & r^3 & r^6 & r^9 \end{pmatrix}, \quad (16)$$

with  $r = e^{2\pi i/4}$  [33]. Hence, the diagonalized shift operator is given as,

$$\Delta = (I \otimes M) S_K (I \otimes M^\dagger) = |0\rangle\langle 0| \otimes \mathcal{R}^\dagger + |1\rangle\langle 1| \otimes \mathcal{R}. \quad (17)$$

QFT is defined on the position space, hence, applies only on the position state of the quantum walker without affecting the coin state. In order to further simplify the implementation of the time evolution operator, one can also express the coin part in terms of the QFT matrices, given as,  $(C \otimes I)$  as  $(I \otimes M^\dagger)(C \otimes I)(I \otimes M)$ .

Exploiting the property  $MM^\dagger = M^\dagger M = I$  results in a quantum circuit that is optimized and efficient by using only one pair of QFT and IQFT operations, the time evolution operator can thus be written as [27],

$$W^t = (I \otimes M^\dagger)[\Delta(C \otimes I)^t(I \otimes M)]. \quad (18)$$

Thus,

$$W^t = (I \otimes M^\dagger)[(|0\rangle\langle 0| \otimes I + |1\rangle\langle 1| \otimes \mathcal{R}^2) \times (C \otimes \mathcal{R}^\dagger)]^t(I \otimes M). \quad (19)$$

We employ the above-described method to devise the cryptographic protocol.

### 1. Steps of the protocol

**1. Generating the chaotic public key.** The initial state of the walker,  $|\Phi_i\rangle = |l\rangle|x\rangle$  and the public key generated by Alice from Eq. (9) is given as,

$$|\Phi_{PK}\rangle = (I \otimes M^\dagger)[(|0\rangle\langle 0| \otimes I + |1\rangle\langle 1| \otimes \mathcal{R}^2) \times (C_B \otimes \mathcal{R}^\dagger)]^2(I \otimes M)|\Phi_i\rangle, \quad (20)$$

where  $W^t = BB$  with  $C_B$  is the coin operator for unitary  $B$ .

**2. Public key transfer.** Alice, after generating the public key, sends it to Bob. This is done via the application of SWAP gates between Alice's and Bob's qubits.

**3. Message Encryption.** To encode the message  $k$ , Bob applies the spatial translation  $T_k$  operator (see, Eq. (11)) to public key  $|\Phi_{PK}\rangle$  with  $T_k$  for different values of  $k \in \{0, 1, 2, 3\}$  in a 4-cycle graph,

$$T_0 = \begin{pmatrix} 1 & 0 & 0 & 0 \\ 0 & 1 & 0 & 0 \\ 0 & 0 & 1 & 0 \\ 0 & 0 & 0 & 1 \end{pmatrix}, \quad T_1 = \begin{pmatrix} 0 & 0 & 0 & 1 \\ 1 & 0 & 0 & 0 \\ 0 & 1 & 0 & 0 \\ 0 & 0 & 1 & 0 \end{pmatrix}, \quad (21)$$

$$T_2 = \begin{pmatrix} 0 & 0 & 1 & 0 \\ 0 & 0 & 0 & 1 \\ 1 & 0 & 0 & 0 \\ 0 & 1 & 0 & 0 \end{pmatrix}, \quad \text{and} \quad T_3 = \begin{pmatrix} 0 & 1 & 0 & 0 \\ 0 & 0 & 1 & 0 \\ 0 & 0 & 0 & 1 \\ 1 & 0 & 0 & 0 \end{pmatrix}.$$

**4. Message transfer.** After encoding the message, Bob transfers it to Alice, which is done again by the SWAP gates applied to Bob's and Alice's qubits.

**5. Message decryption.** As Bob encodes the message, Alice applies the decryption operator  $G = (AABB)^4AA$ , since  $(AABB)^5 = I$  (Parrondo sequence with periodicity 20) [20], the final state has the form after two pairs QFTs

and IQFTs, one pair while generating the public key and the other pair decrypting the message. The final state is,

$$|\Phi_f\rangle = (I \otimes M^\dagger)[(|0\rangle\langle 0| \otimes I + |1\rangle\langle 1| \otimes \mathcal{R}^2)(C_G \otimes \mathcal{R}^\dagger)] \times (I \otimes M)(I \otimes T_k)(I \otimes M^\dagger)[(|0\rangle\langle 0| \otimes I + |1\rangle\langle 1| \otimes \mathcal{R}^2)(C_B \otimes \mathcal{R}^\dagger)]^2(I \otimes M)|\Phi_i\rangle, \quad (22)$$

$C_G$  being the coin operator associated with unitary  $G$ . We note that the  $T_k$  operators are the same as the shift operators. Hence, they too can be diagonalized by QFT (IQFT) matrices. This lets us use the unitarity condition,  $M^\dagger M = I$ , and one can have an efficient implementation with a single pair QFT and one IQFT. The diagonalized  $T_k$  operator is given as,

$$T_k^D = M^\dagger T_k M, \quad (23)$$

where  $T_k^D$  is the diagonalized form of  $T_k$  which is given as,

$$T_0^D = \begin{pmatrix} 1 & 0 & 0 & 0 \\ 0 & 1 & 0 & 0 \\ 0 & 0 & 1 & 0 \\ 0 & 0 & 0 & 1 \end{pmatrix} = \begin{pmatrix} 1 & 0 \\ 0 & 1 \end{pmatrix} \otimes \begin{pmatrix} 1 & 0 \\ 0 & 1 \end{pmatrix},$$

$$T_1^D = \begin{pmatrix} 1 & 0 & 0 & 0 \\ 0 & i & 0 & 0 \\ 0 & 0 & -1 & 0 \\ 0 & 0 & 0 & -i \end{pmatrix} = \begin{pmatrix} 1 & 0 \\ 0 & -1 \end{pmatrix} \otimes \begin{pmatrix} 1 & 0 \\ 0 & i \end{pmatrix},$$

$$T_2^D = \begin{pmatrix} 1 & 0 & 0 & 0 \\ 0 & -1 & 0 & 0 \\ 0 & 0 & 1 & 0 \\ 0 & 0 & 0 & -1 \end{pmatrix} = \begin{pmatrix} 1 & 0 \\ 0 & 1 \end{pmatrix} \otimes \begin{pmatrix} 1 & 0 \\ 0 & -1 \end{pmatrix}, \quad \text{and}$$

$$T_3^D = \begin{pmatrix} 1 & 0 & 0 & 0 \\ 0 & -i & 0 & 0 \\ 0 & 0 & -1 & 0 \\ 0 & 0 & 0 & i \end{pmatrix} = \begin{pmatrix} 1 & 0 \\ 0 & -1 \end{pmatrix} \otimes \begin{pmatrix} 1 & 0 \\ 0 & -i \end{pmatrix}. \quad (24)$$

Eq. (24) enables us to encode the message via single-qubit phase rotation gates ( $P(\theta)$ ) i.e.,

$$P(\theta) = \begin{pmatrix} 1 & 0 \\ 0 & e^{i\theta} \end{pmatrix}. \quad (25)$$

The diagonalized  $T_k$ 's are thus,

$$T_0 = I \otimes I, \quad T_1 = P(\pi) \otimes P(\pi/2), \quad (26)$$

$$T_2 = I \otimes P(\pi), \quad \text{and} \quad T_3 = P(\pi) \otimes P(-\pi/2).$$

In this work, we propose a module-based quantum cryptography protocol, where communication is modeled through the transfer of quantum states across virtual modules of a quantum processor. Instead of relying on physically separate devices, Alice and Bob are assigned disjoint sets of qubits that act as their respective modules. The exchange of information is simulated using SWAP operations between these registers, enabling the

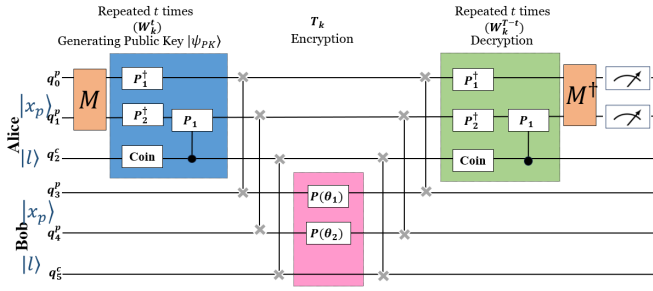


FIG. 1. Schematic representation of the quantum circuit of the quantum cryptographic protocol.

preparation, transmission, and recovery of encoded messages entirely within a single NISQ device. Alice begins with three qubits  $q_0, q_1, q_2$  (for 4-cycle graph), which serve as her position and coin registers. She prepares the initial state by applying coin rotations and conditional shift operators, generating her public key state distributed over these virtual modules. To hand over the state to Bob, Alice uses a sequence of SWAP gates to transfer her prepared qubits into Bob's register ( $q_3, q_4, q_5$ ). This mimics the physical transmission of a quantum state across a communication channel while remaining entirely within the same quantum processor. Bob encodes his message  $k$  through spatial translations (application of  $T_k$  operator). After encoding, Bob again uses SWAP gates to send the modified quantum state back to Alice's registers. With the state returned to her qubits, Alice applies the decryption operator, which is the inverse of her initial public-key operation. Alice then measures her position qubits in the computational basis to read out the message. The schematic representation of the complete protocol is depicted in Fig. 1.

#### IV. RESULTS

To implement the proposed cryptographic protocol, we employ the Parrondo strategy in  $AABB\dots$  sequence on a 4-cycle graph, using the parameters for  $A$  and  $B$  as defined in section II. The quantum circuit, illustrated in Fig. 1, is first simulated using Qiskit's `AerSimulator()` to obtain ideal results. Subsequently, noisy simulations are performed with Qiskit's `NoiseModel()`.

To quantify the similarity between the probability distributions obtained from ideal and noisy discrete-time quantum walk (DTQW) simulations, we employ the *Hellinger fidelity*. Let  $X = \{x_i\}$  and  $Y = \{y_i\}$  denote two discrete probability distributions, where  $X$  corresponds to the distribution obtained from ideal simulations (e.g., using `AerSimulator()`) and  $Y$  represents the distribution obtained in the presence of noise. The Hellinger fidelity [34, 35] between  $X$  and  $Y$  is formulated as,

$$H(X, Y) = [1 - h^2(X, Y)]^2, \quad (27)$$

with  $h$  denoting the Hellinger distance defined as,

FIG. 2. **Algorithm 1:** Parrondo's Paradox cyclic QW based Cryptographic Protocol on a 4-cycle graph (see, Fig. 1)

```

1: Input: Coin operators  $A, B$  generating chaotic DTQW dynamics
2: Design the circuit with 6 qubits: Alice 3 qubits  $q_0q_1q_2$ , Bob 3 qubits  $q_3q_4q_5$ ; Position qubits:  $q_0q_1, q_3q_4$ , Coin qubits:  $q_2$  and  $q_5$ 
Public Key Generation by Alice
3: Initialize  $q_0q_1q_2$ 
4: Apply QFT on position qubits of Alice  $q_1q_0$ 
5: Apply SWAP on  $q_1q_0$  to get the correct output
6: for  $i = 0$  to 2 do
7:   Perform the coin operation  $B$  on  $q_2$ 
8:   Perform the phase rotation  $P(-\pi)$  on  $q_0$ 
9:   Perform the phase rotation  $P(-\pi/2)$  on  $q_1$ 
10:  if  $|q_2\rangle$  is in  $|1\rangle$  then
11:    Perform the phase rotation  $P(\pi)$  on  $q_1$ 
12:  end if
13: end for
Public Key transfer from Alice to Bob
14: Perform the SWAP gates to swap Alice's qubits with Bob's
Message Encryption by Bob
15: Encrypt the message via  $T_k^D$  operator on Bob's position qubits  $q_3q_4$ 
Message transfer from Bob to Alice
16: Apply SWAP gates to swap Bob's qubits with Alice
Message decryption by Alice
17: for  $i = 0$  to 18 do
18:  if  $i \bmod 4 = 0$  or  $i \bmod 4 = 1$  then
19:    Perform the coin operation  $A$  on  $q_2$ 
20:  else
21:    Perform the coin operation  $B$  on  $q_2$ 
22:  end if
23:  Perform the phase rotation  $P(-\pi)$  on  $q_0$ 
24:  Perform the phase rotation  $P(-\pi/2)$  on  $q_1$ 
25:  if  $|q_2\rangle$  is in  $|1\rangle$  then
26:    Perform the phase rotation  $P(\pi)$  on  $q_1$ 
27:  end if
28: end for
29: Apply SWAP on  $q_1q_0$  to get the correct output
30: Apply IQFT on position qubits  $q_1q_0$ 
31: Alice measures her position qubits  $q_1q_0$ 

```

$$h(X, Y) = \frac{1}{\sqrt{2}} \sqrt{\sum_i (\sqrt{x_i} - \sqrt{y_i})^2}. \quad (28)$$

The *Hellinger fidelity* takes values in the interval  $[0, 1]$ , where a value of 1 indicates identical probability distributions, while 0 corresponds to completely distinguishable distributions. Fidelity values exceeding 0.5 signify a strong similarity between the distributions, whereas values above 0.95 indicate near-perfect agreement. Since our analysis focuses on the dynamics of the probability distributions of the position states, the Hellinger fidelity serves as a natural and meaningful metric to quantify the closeness between the probability distributions acquired from ideal and noisy simulations performed using

`qiskit_aer`.

In addition to the Hellinger fidelity, one may also evaluate the total variation distance, which measures the statistical distinguishability between two probability distributions by quantifying the maximum difference in the probabilities that each distribution assigns to the same events. For probability distributions  $X = \{x_i\}$  and  $Y = \{y_i\}$ , the total variation distance is given by

$$T(X, Y) = \frac{1}{2} \sum_k |x_i - y_i|. \quad (29)$$

The total variation distance is bounded by  $[0, 1]$ , where 0 indicates the distributions are similar, while 1 means that they are completely different.

Fig. 3 shows the probability distribution during the public key generation of the cryptographic protocol, with the walker initialized at  $|0\rangle$  position state and  $|l\rangle = |0\rangle$  coin state. The results show the circuit realizations both in ideal conditions and with realistic quantum noise using Qiskit's noise modeling framework. Gate imperfections are modeled by a depolarizing quantum channel with an error probability of 0.03 applied uniformly to all quantum gates in the circuit. The depolarizing channel provides an effective description of averaged gate errors arising from control inaccuracies, crosstalk, and residual decoherence, and is commonly used to benchmark quantum algorithms on NISQ devices. The chosen error probability closely reflects the effective noise levels observed on current-generation IBM superconducting quantum processors [36] operated at optimization level 3. This approach allows us to capture the aggregate influence of gate noise on the quantum walk dynamics and the resulting cryptographic performance. The close similarity between the ideal and noisy probability distributions indicates that the protocol is stable and that noise has only a small effect on the quantum walk dynamics. This means that the public key can be generated accurately even on the current generation noisy intermediate-scale quantum (NISQ) hardware. For completeness, the quantum circuits implementing the protocol are presented in Appendix A. In addition to the Qiskit-based simulations presented above, we also provide a proof-of-principle implementation of the complete cryptographic protocol using the `Wolfram Quantum Framework` [37] in Mathematica. The corresponding results of the ideal and noisy simulations are reported in Appendix B.

Fig. 4 presents the decrypted messages obtained when the quantum circuits are realized with and without noise, with nearly 80% Hellinger fidelity (see, Fig. 5) for all the messages. Additionally, Fig. 6 shows that the messages encoded using different initial walker states can also be reliably decrypted, with Hellinger fidelity, 80%, and total variation distance, 20%, further demonstrating the robustness and correctness of our circuit design. The slightly reduced fidelity observed in the noisy simulations can be understood as a consequence of how the protocol is realized at the circuit level. The encryption-decryption process involves several sequential operations, including

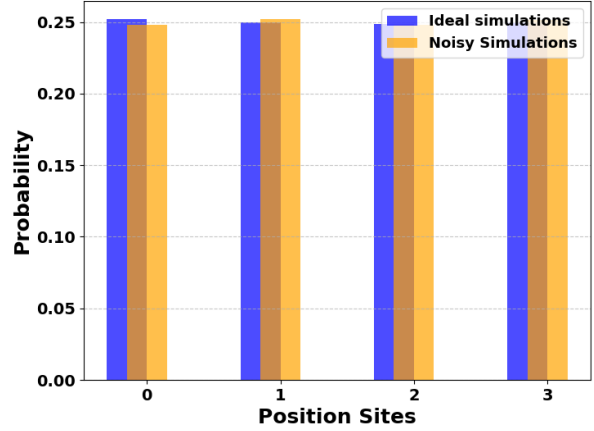


FIG. 3. Probability distribution for the public key generation on a 4-cycle graph with initial position  $|x\rangle = |0\rangle$  and  $|l\rangle = |0\rangle$  implemented in `qiskit_aer` with (0.03 depolarizing) and without noise for  $10^5$  shots.

repeated SWAP gates used to transfer quantum states between the virtual modules representing Alice and Bob. These additional operations increase the overall circuit depth, allowing noise to accumulate over the course of the computation. On real quantum hardware, such state transfers typically correspond to larger physical separations between qubits and limited connectivity, which further amplify gate errors. As a result, the final probability distribution becomes more spread out. Importantly, the fidelity remaining close to 80% indicates that the underlying periodic revival of the quantum walk is largely preserved, enabling reliable message recovery despite realistic noise levels.

## V. SECURITY OF THE PROTOCOL

### A. Intercept and Resend Attack

In quantum communication protocols, the security of information exchange between two legitimate parties, Alice and Bob, relies on the fundamental principles of quantum mechanics. However, an adversary, commonly referred to as Eve, may attempt to gain unauthorized access to the transmitted quantum states. One of the most basic yet impactful strategies employed by Eve is the intercept-and-resend attack [29].

In this attack model, Eve intercepts the quantum states sent from Alice to Bob, performs measurements on them, and then prepares and sends new quantum states to Bob that mimic the original as closely as possible. By doing so, Eve attempts to extract information about the secret data or key being exchanged, while minimizing the disturbance introduced into the system. Since quantum states cannot, in general, be measured without altering

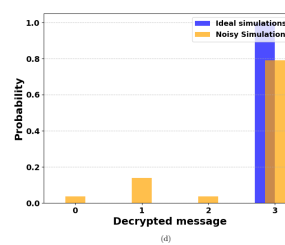
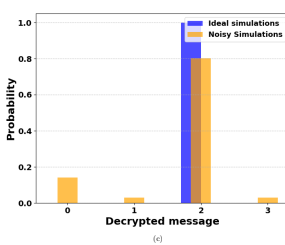
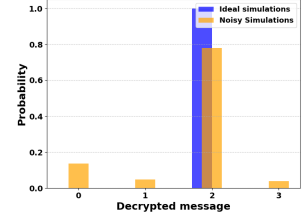
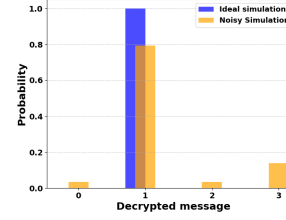
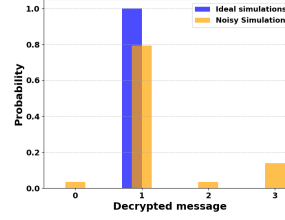
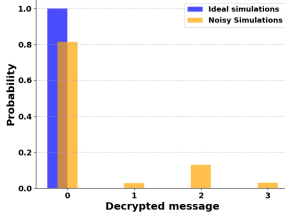


FIG. 4. Probability distribution for the Decrypted message,  $k'$  for encoded message (a)  $k = 0$ , (b)  $k = 1$ , (c)  $k = 2$ , (d)  $k = 3$  with initial position  $|x\rangle = |0\rangle$  such that  $k' = k$  implemented in `qiskit_aer` with depolarizing noise and without noise for  $10^5$  shots on a 4-cycle graph.

FIG. 6. Probability distribution for the Decrypted message,  $k'$  for encoded message  $k = 1$  for different initial position (a)  $|x\rangle = |0\rangle$ , (b)  $|x\rangle = |1\rangle$ , (c)  $|x\rangle = |2\rangle$ , and (d)  $|x\rangle = |3\rangle$  such that  $k' = (k + x) \bmod N$ , with  $l \in \{0, 1, 2, 3\}$  implemented in `qiskit_aer` with depolarizing noise and without noise for  $10^5$  shots on a 4-cycle graph.

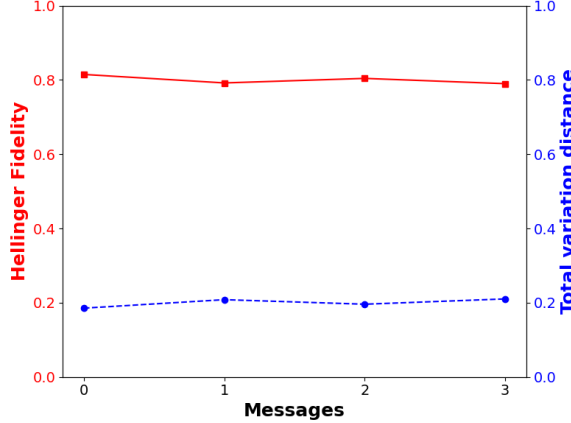


FIG. 5. Hellinger Fidelity and total variance distance for different messages decrypted by Alice with initial position  $|x\rangle = |0\rangle$  and coin  $|s\rangle = |0\rangle$  implemented in `qiskit_aer` with depolarizing noise and without noise for  $10^5$  shots on a 4-cycle graph.

them, Eve's intervention inevitably introduces detectable errors in the communication channel. The appearance of such anomalies alerts Alice and Bob to the presence of eavesdropping.

On the security of our cryptographic protocol, let us consider the DTQW on a 4-cycle graph such that the position state be  $|x\rangle = |00\rangle$  (i.e., site  $|K = 0\rangle$ ), and coin state  $|l\rangle = |0\rangle$  initially, and the message is, say,  $k = 1$ . An eavesdropper can attack at step 3 (stages 12-13 see, Algorithm 1 (Fig. 2) when Bob sends the encrypted and encoded message  $|\Phi(k)\rangle$  to Alice. Since Eve does not know the private key, Eve learning the state  $|\Phi(k = 1)\rangle$  is al-

most impossible (i.e., it has negligible probability). This mitigates an intercept-and-resend attack wherein Eve can try to measure Alice's signal or the message-encrypted state. To assess the security of the protocol at the circuit level, we introduce an eavesdropper, Eve, equipped with three qubits analogous to the modules used by Alice and Bob. Eve is then incorporated into the communication process, enabling us to simulate an intercept-and-resend attempt within the same computational framework. By executing the protocol in the presence of Eve and tracking the resulting state evolution, we can evaluate how effectively the cryptographic scheme detects and resists unauthorized interference. The complete algorithm demonstrating the protocol's security under this attack model is presented in Algorithm 2 (Fig. 8).

To quantify the effect of Eve's intercept-and-resend attack, we evaluate the Quantum Bit Error Rate (QBER), defined here as the probability that Alice's decrypted message differs from the correct value. For our DTQW-based protocol, QBER [38] is computed as,

$$\text{QBER} = 1 - P(k), \quad (30)$$

where  $P(k)$  is the probability (from the final position-state distribution) that Alice recovers the correct message. QBER is bounded in the interval  $[0, 1]$ , where a value of 0 indicates error-free message recovery and a value of 1 corresponds to complete failure of decryption. Exact decryption in the proposed protocol relies on the periodic revival of the quantum walk under the private Parrondo sequence. In the presence of Eve, the collapse of the walk's periodic structure spreads the probability across all position states, sharply decreasing the proba-

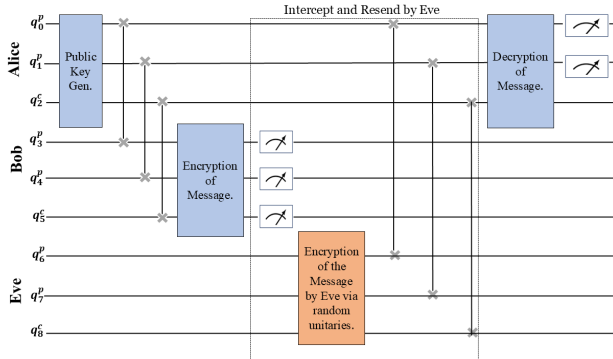


FIG. 7. Schematic representation of the quantum circuit in the presence of Eve performing an intercept and resend attack on the quantum cryptographic protocol.

bility of getting the correct message and yielding a high QBER. Thus, QBER serves as a clear indicator of Eve's interference in intercept-and-resend attacks. A schematic representation of the quantum circuit with Eve performing an intercept and resend attack is depicted in Fig. 7.

Fig. 9 (a) presents the probability distribution of the decrypted message obtained by Alice with Eve performing an intercept and resend attack on the encoded message  $k = 1$ . The results from both ideal and noisy simulations show that measurement outcomes are widely dispersed across all possible decrypted messages rather than concentrated around the correct value. Instead of recovering the message  $k' = 1$  (see Fig. 4), the presence of Eve causes Alice's subsequent decryption to yield a mixed distribution over all message values, indicating that the original message information is effectively lost as a result of Eve's interference. This mixture ensures that Eve's attempt not only fails to reveal the encoded message but also introduces detectable disturbances in the communication process. The noisy simulation further broadens this distribution, reinforcing the conclusion that Eve gains no advantage even in non-ideal environments. Overall, this confirms that the protocol is intrinsically secure against intercept-and-resend attacks. Eve's intrusion transforms the decrypted outcome into a mixture of all possible messages, ensuring both message confidentiality and attack detectability. Also, Eve's measurement causes the probability at the correct outcome to drop to a very small value (ideal-0.04 and noisy - 0.08) while the remaining probability mass spreads uniformly across the incorrect messages. Consequently, the QBER rises close to its maximal value (ideal-0.96 and noisy-0.92), indicating that Alice almost never recovers the correct message when Eve intervenes. This extremely high QBER (see Fig. 9 (b)) confirms that any intercept-and-resend attempt produces a strong, unambiguous disturbance in the decrypted outcomes, making the attack immediately detectable. The corresponding circuit realizations used in the security analysis are included in Appendix A.

FIG. 8. **Algorithm 2:** Intercept and Resend Attack on 4-cycle graphs (see, Fig. 7)

```

1: Input: Coin operators  $A$ ,  $B$  generating chaotic DTQW dynamics
2: Design the circuit with 9 qubits: Alice 3 qubits  $q_0q_1q_2$ , Bob 3 qubits  $q_3q_4q_5$ , and Eve 3 qubits  $q_6q_7q_8$ . Position qubits for Alice are  $q_0q_1$ , for Bob are  $q_3q_4$ , and for Eve are  $q_6q_7$ . Coin qubits: Alice  $q_2$ , Bob  $q_5$ , and Eve  $q_8$ 
Public Key Generation by Alice
3: Initialize  $q_0q_1q_2$ 
4: Apply QFT on position qubits of Alice  $q_1q_0$ 
5: Apply SWAP on  $q_1q_0$  to get the correct output
6: for  $i = 0$  to 2 do
7:   Perform the coin operation B on  $q_2$ 
8:   Perform the phase rotation  $P(-\pi)$  on  $q_0$ 
9:   Perform the phase rotation  $P(-\pi/2)$  on  $q_1$ 
10:  if  $|q_2\rangle$  is in  $|1\rangle$  then
11:    Perform the phase rotation  $P(\pi)$  on  $q_1$ 
12:  end if
13: end for
Public Key transfer from Alice to Bob
14: Apply SWAP gates to swap Alice's qubits with Bob's
Message Encryption by Bob
15: Encrypt the message via the  $T_k^D$  operator to Bob's position qubits  $q_3q_4$ 
Interception by Eve
16: Eve measures Bob's qubits by applying random (computational or X basis) measurement operators
17: Eve encodes the message based on her measurements via random unitary matrices on qubits  $q_6q_7q_8$ 
Message transfer by Eve
18: Apply SWAP gates to swap Eve's qubits with Alice's
Message decryption by Alice
19: for  $i = 0$  to 18 do
20:  if  $i \bmod 4 = 0$  or  $i \bmod 4 = 1$  then
21:    Perform the coin operation A on  $q_2$ 
22:  else
23:    Perform the coin operation B on  $q_2$ 
24:  end if
25:  Perform the phase rotation  $P(-\pi)$  on  $q_0$ 
26:  Perform the phase rotation  $P(-\pi/2)$  on  $q_1$ 
27:  if  $|q_2\rangle$  is in  $|1\rangle$  then
28:    Perform the phase rotation  $P(\pi)$  on  $q_1$ 
29:  end if
30: end for
31: Apply SWAP on  $q_1q_0$  to get the correct output
32: Apply IQFT on position qubits  $q_1q_0$ 
33: Alice measures her position qubits  $q_1q_0$ 

```

## B. Man-in-the-middle Attack

The man-in-the-middle attack [29] functions as an authentication check, where Alice verifies whether the incoming quantum state genuinely originates from Bob or has been tampered with by an adversary such as Eve. Bob and Alice share a pre-established private key, the Parrondo sequence that ensures the walk evolves periodically during decryption. If Eve attempts to intercept, modify, or replace the transmitted state, she inevitably applies operations that break the periodicity. Conse-

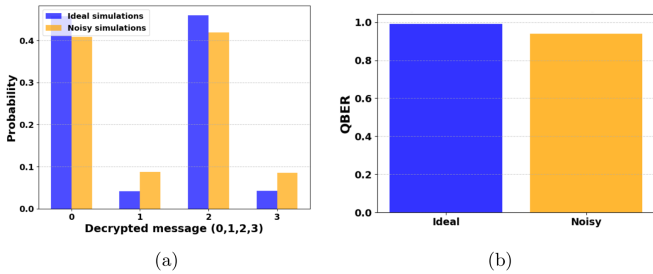


FIG. 9. (a) Probability Distribution for the Decrypted message  $k'$ , intercepted by Eve for encoded message  $k = 1$  with initial position  $|x\rangle = |0\rangle$  such that  $k' = k$  implemented in `qiskit.aer` with depolarizing noise and without noise for  $10^5$  shots. (b) Quantum bit error rate (QBER) obtained in ideal and noisy simulations for the cryptographic protocol intercepted by Eve.

quently, when Alice performs the inverse Parrondo sequence during decryption, the resulting position distribution fails to match the expected periodic revival, immediately signalling Eve's presence. Additionally, the probability of any Eve guessing the correct decryption operator  $G$  retracing back to the quantum state is practically negligible because there exist infinitely many ways to form coin operators, and their combinations for the DTQW evolution. The private key information is inaccessible to Eve, and she has almost zero probability of knowing Bob's encrypted quantum state  $|\Phi(k)\rangle$ . Furthermore, the chaotic dynamics in the public key ( $|\Phi_{PK}\rangle$ ) add another layer of protection by producing a highly sensitive, interference-dominated quantum state that is effectively impossible to invert or replicate without knowledge of the exact Parrondo sequence.

## VI. ANALYSIS

The results presented in the previous section demonstrate that our DTQW-based cryptographic protocol performs reliably under ideal and noisy conditions, and exhibits a very strong disturbance signature under intercept-and-resend attacks. To appreciate the significance of this behavior from a broader quantum-cryptographic perspective, it is useful to relate our findings to what is typically expected from a standard prepare-and-measure protocol. BB84 is the most widely recognized example of such a scheme, and serves as a conventional benchmark for how noise and eavesdropping reveal themselves through quantum state disturbance. Although our protocol operates on fundamentally different principles and does not incorporate BB84 in any step of its construction, using BB84 here purely as a reference allows us to contextualize the strength of the disturbance observed in our results.

Table I compares the performance of BB84 protocol and our proposed Parrondo's paradox-based DTQW protocol obtained from simulations of both schemes under (i)

Scenario	BB84 [1]	Parrondo DTQW
Ideal (no Eve)	$\approx 0$	$\approx 0$
Eve intercept-resend	$\approx 0.25$	0.92
Authentication	Needs extra classical channel	Inherent (Private key)

TABLE I. Comparison between BB84 and the proposed Parrondo's paradox-based DTQW protocol based on QBER values

ideal conditions, and (ii) a full intercept-and-resend attack. To establish a baseline, we simulated the BB84 protocol using a single-qubit prepare-and-measure scheme in Qiskit. In the ideal case, the sifted keys obtained by Alice and Bob match perfectly, resulting in a QBER  $\approx 0$ . The sifted key is formed after Alice and Bob publicly compare their measurement bases and retain only those bits for which compatible bases were used, discarding the rest. Under an intercept-and-resend attack, Eve collapses the prepared quantum state by measuring it in a randomly chosen basis and resending her outcome. This induces a well-known disturbance of approximately 0.25 in the sifted key. Our implementation reproduces this behavior, confirming that BB84 detects eavesdropping statistically through a characteristic but relatively mild increase in QBER. This detection requires a sufficiently large number of transmitted qubits for reliable estimation. The results of our proposed protocol demonstrate a qualitatively different behavior. The periodic evolution reliably recovers the encrypted messages with high success probability. The most notable effect appears when Eve attempts an intercept-and-resend attack. By performing a measurement, Eve collapses the multi-amplitude quantum-walk state and is unable to reproduce the private coin dynamics. Consequently, Alice's decryption no longer yields peaked distributions; instead, it approaches a near-uniform output. The probability of recovering the correct message falls to approximately 0.04–0.08 (see, Fig. 9 (a)), corresponding to QBER values in the range 0.92–0.96 (see, Fig. 9 (b)), which is dramatically higher than BB84's 0.25. Thus, any adversarial intervention results in almost total failure of decryption, enabling immediate and unmistakable detection without the need for statistical sampling. In addition, the BB84 protocol does not have native authentication. To authenticate the legitimate communicating parties, an additional classical channel is required, whereas our proposed protocol ensures intrinsic authentication, enabling secure message transfer and instantaneous eavesdropper detection from a single experimental run rather than relying on statistical averaging over long keys.

## VII. NISQ IMPLEMENTATION: RESULTS AND CHALLENGES

The proposed Parrondo's paradox-based cryptographic protocol was implemented and tested on IBM's

superconducting quantum computing platform using the `ibm_torino` backend, a 133-qubit quantum device based on the *Heron r1* processor, accessed via IBM Quantum cloud services [36]. Realizing the proposed protocol on present-day NISQ hardware presents several practical challenges that arise from limited qubit connectivity, hardware noise, and transpiler-induced circuit transformations [31]. In principle, the protocol assumes that Alice and Bob reside on spatially separated quantum processors and exchange quantum states over a communication channel. Since such distributed quantum computation is not yet reliably supported on current NISQ hardware [32], we emulated this setting on a single processor by assigning disjoint and widely separated qubit modules to Alice and Bob. In our implementation, Alice and Bob were mapped to distant registers, thereby maximizing logical separation as detailed in Appendix C. A primary challenge stems from quantum state transfer between distant qubit modules. Quantum state transfer between Alice and Bob was realized via sequences of SWAP operations across intermediate qubits. This leads to a substantial increase in circuit depth and, consequently, significant error accumulation. Moreover, at higher transpiler optimization levels, aggressive qubit remapping and gate reordering can partially or entirely erase the intended modular separation between Alice and Bob, resulting in a loss of distinction between the communicating parties and undermining the cryptographic structure of the protocol (see, Appendix C1). To mitigate these limitations, we explored hybrid quantum state-transfer strategies combining SWAP operations with quantum teleportation, which more closely resemble a distributed communication paradigm while preserving logical modularity. As shown in Appendix C2, these hybrid approaches can better maintain the Alice–Bob separation enforced at the circuit level. However, teleportation introduces its own sources of error through Bell-pair generation, additional entangling gates, and measurement operations. Consequently, the relative performance of SWAP-then-teleport versus teleport-then-SWAP strategies is found to depend sensitively on the specific choice of physical qubits, their connectivity, and local error rates.

Overall, these results demonstrate that the protocol performance is governed by a trade-off between circuit depth, noise accumulation, and preservation of logical communication structure. The findings underscore the necessity of hardware-aware qubit selection and communication ordering when implementing cryptographic protocols on current quantum processors and motivate our simulation-based, proof-of-principle validation. Although this limitation prevented an experimental demonstration on distributed hardware, recent advances toward modular quantum architectures [39] represent promising steps toward fully distributed implementations in the future.

## VIII. CONCLUSION

Periodic quantum walks can be used to design a quantum cryptographic protocol, where Parrondo sequences combine individually chaotic operators to obscure the walk dynamics while still allowing periodic revivals to be recovered with the correct sequence. Consequently, the encryption stage generates a highly delocalized quantum state, and successful decryption depends on applying the precise unitary sequence that restores periodicity. Building on this idea, we propose an explicit quantum circuit realization of DTQW-based cryptographic protocol that is compatible with the current generation gate-based NISQ hardware [36]. Given the current limitations of NISQ hardware, which do not yet support implementations across physically separated quantum processors, we realize the protocol on a single quantum processor by assigning disjoint qubit modules to represent the communicating parties, with Alice as the receiver and Bob being the sender. We analyze the performance of the protocol through numerical simulations carried out in Qiskit under both ideal conditions and in the presence of depolarizing noise. In the noiseless case, the periodic revival structure of the walk is faithfully recovered, leading to high agreement between the decrypted and original probability distributions. When depolarizing noise is included, the recovered distributions deviate from the ideal case, which is quantitatively reflected by Hellinger fidelity ( $\approx 80\%$ ) and the total variation distance ( $\approx 20\%$ ). These deviations arise from accumulated gate errors and state-transfer operations inherent to the circuit implementation. The security of the protocol arises from encoding the message onto a chaotic public key generated by the DTQW. In the circuit implementation, this public key corresponds to a chaotic unitary evolution, making the encoded state highly sensitive to interference. Any action by an eavesdropper alters the implemented gate sequence and leads to observable deviations in the decrypted statistics. In contrast, successful authentication requires the application of the exact decryption operator, implemented as a specific Parrondo sequence of coin operations. This operator acts as a private key by reconstructing the periodic revival of the walk. By explicitly modeling intercept-and-resend and man-in-the-middle attacks within the quantum circuit framework, we showed that adversarial intervention disrupts the periodic revival mechanism, leading to a pronounced increase in QBER ( $\approx 92\%$ ) and a clear statistical signature of interference. These results indicate that the protocol exhibits strong disturbance sensitivity at the circuit level. We further corroborate our findings through independent simulations in the Wolfram Quantum Framework (Mathematica), ensuring platform-independent validation of the protocol dynamics (detailed in Appendix B). Our study also highlights the practical challenges associated with implementing the protocol on the quantum hardware. As detailed in Appendix C, state transfer realized solely through SWAP

operations introduces significant limitations. At higher transpiler optimization levels, the logical distinction between communicating parties is compromised, whereas at lower optimization levels the increased circuit depth leads to reduced fidelity. To address these constraints, we investigate hybrid state-transfer strategies that combine SWAP operations with quantum teleportation. While this approach improves overall protocol performance, it remains sensitive to the choice of physical qubits and the underlying qubit connectivity of the device.

While this manuscript focuses on small cyclic graphs,

the framework can be extended to larger systems and more realistic hardware-specific error channels. Exploring the implementation on physically distributed quantum processors, optimization of state-transfer strategies, and analysis under more general adversarial models mark an important direction for future study. More broadly, this work demonstrates that dynamical phenomena intrinsic to quantum walks, rather than entanglement or basis randomness alone, can serve as the foundation for secure, circuit-level quantum cryptographic protocols in the near term quantum devices.

## Appendix A: Quantum circuit realizations in QISKit

Herein, we present the explicit quantum circuits used to implement and verify the Parrondo’s paradox-based cryptographic protocol within the Qiskit framework. The circuits shown here correspond to the building blocks and full protocol discussed in Sec. III B and are provided to ensure transparency and reproducibility of the results reported in Secs. IV and V. All circuits are constructed using a gate-based model suitable for near-term NISQ devices. For a 4-cycle graph, the DTQW is encoded using three qubits: two qubits represent the position space, while one qubit denotes the coin degree of freedom. As described earlier (see, Sec. VII), we implement the protocol with Alice and Bob as separate modules in a single quantum processor. In the module-based cryptographic implementation, Alice and Bob are each assigned independent three-qubit registers, and communication between them is modeled using SWAP operations within a single quantum processor.

Fig. 10 illustrates the two fundamental circuit components used in the cryptographic protocol. Fig. 9(a) shows the public key generation step implemented by Alice, where the initial walker state is evolved through successive applications of the chaotic coin operator  $B$ , following the DTQW dynamics described in Sec. III. This operation generates the public key that is subsequently shared with Bob. Fig. 9(b) depicts the decryption operator  $G$  employed by Alice to recover Bob’s encrypted message. The operator  $G$  corresponds to the deterministic Parrondo sequence  $(AABB)^4AA$  implemented as a sequence of DTQW steps.

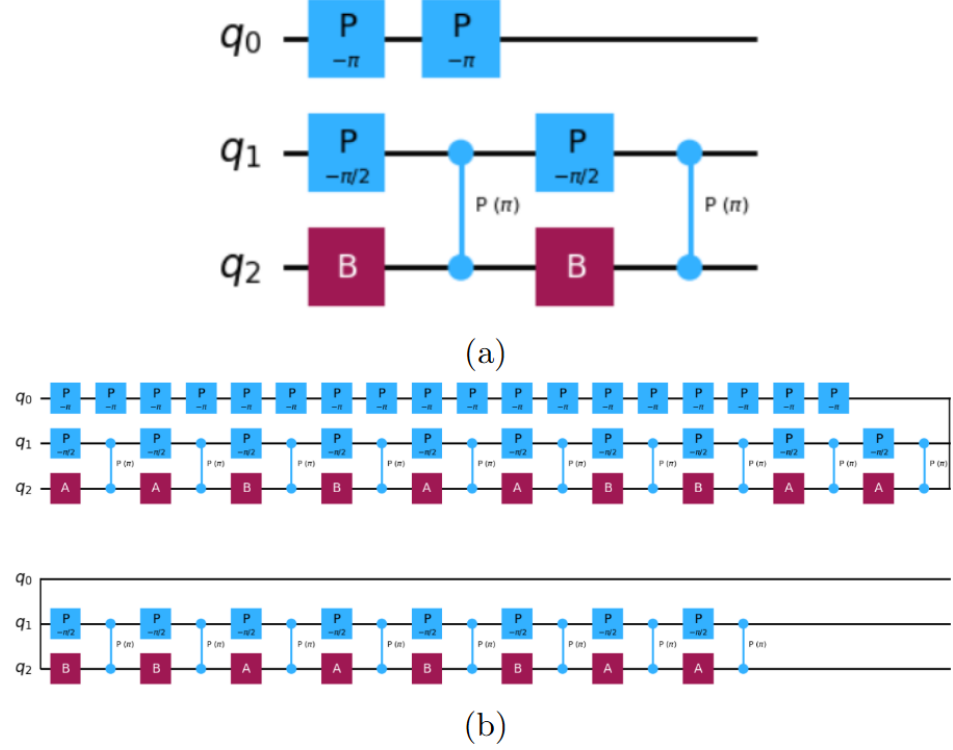


FIG. 10. Quantum circuits for (a) Public Key generated by Alice ( $|q_0q_1q_2\rangle$ ) and (b) Decryption operator  $G = (AABB)^4AA$  applied by Alice to recover the message encrypted by Bob.

Fig. 11 shows the complete quantum circuit implementing the proposed cryptographic protocol. The circuit incorporates public key generation, message encoding by Bob, state transfer between Alice and Bob, and the subsequent decryption performed by Alice.

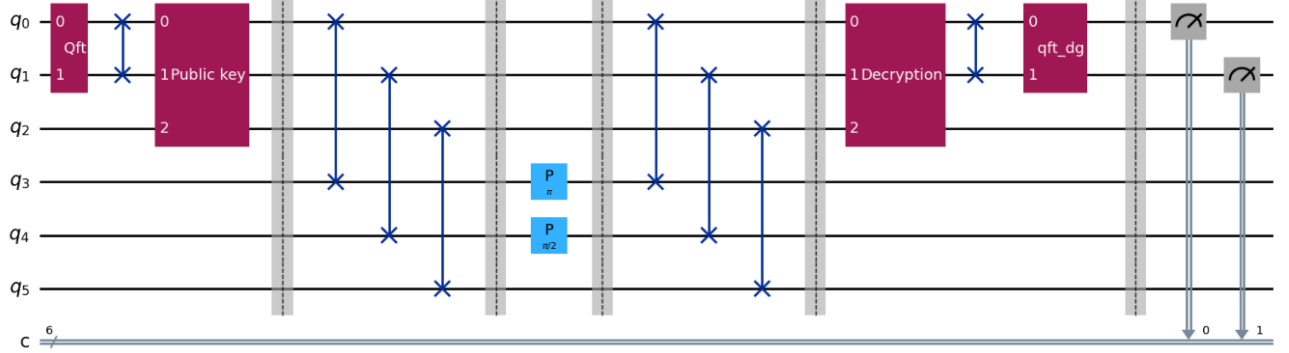


FIG. 11. Quantum circuit implementing the proposed Parrondo's paradox-based cryptographic protocol. Qubits  $q_0, q_1$  and  $q_2$  represent Alice's position and coin degrees of freedom, while qubits  $q_3, q_4$  and  $q_5$  correspond to Bob's register. The circuit realizes public key generation by Alice with initial state  $|000\rangle$ , message  $k = 1$  encoding by Bob, state transfer between the parties, and subsequent decryption performed by Alice.

Fig. 12 presents the extended circuit used to simulate adversarial behavior, where an additional three-qubit register is assigned to Eve. This circuit realizes an intercept-and-resend attack by allowing Eve to measure, re-encode, and forward the quantum state to Alice. The resulting disruption of the walk's periodicity is directly observable in the decrypted probability distributions and forms the basis of the security analysis discussed in Sec. V.

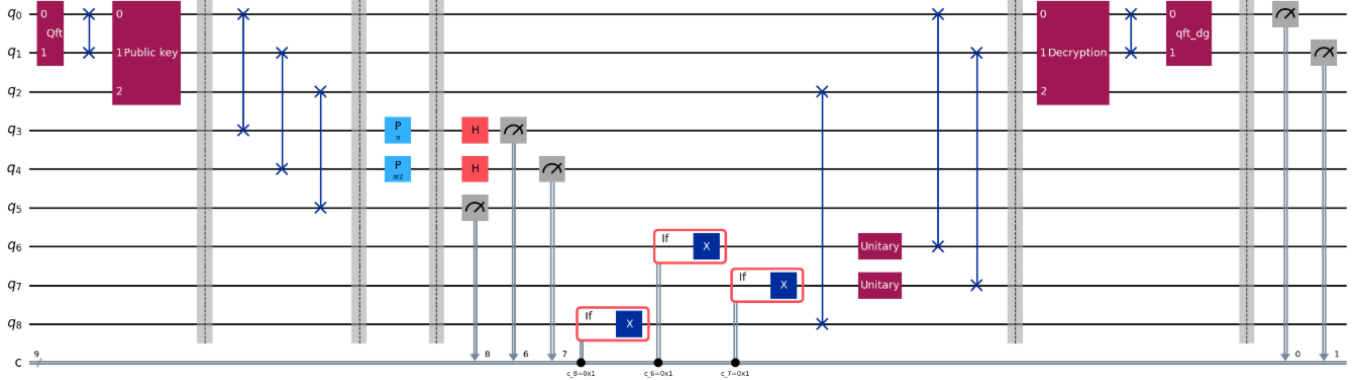


FIG. 12. Quantum circuit implementing the proposed Parrondo’s paradox-based cryptographic protocol in the presence of an adversary Eve. Qubits  $q_0, q_1$  and  $q_2$  represent Alice’s position and coin degrees of freedom, while qubits  $q_3, q_4$  and  $q_5$  correspond to Bob’s register and qubits  $q_6, q_7$  and  $q_8$  correspond to Eve.

All circuits were simulated using Qiskit Aer under both ideal conditions and with realistic depolarizing noise models, as described in Sec. IV. The appendix figures thus serve as a circuit-level reference for the numerical simulations and security analysis presented in the main text. The codes supporting the plots of the main text are available in Ref. [40].

## Appendix B: Quantum Circuit Realization and Simulation in Mathematica

In addition to the Qiskit-based implementation presented in the main text, we independently realized and simulated the Parrondo’s paradox-based quantum cryptographic protocol using the **Wolfram Quantum Framework** [37] in Mathematica.

In the Qiskit framework, realistic noise is modeled by applying noise channels to individual unitary gates, closely mimicking hardware-level gate imperfections. In contrast, the Mathematica simulations implement noise as an effective qubit-level process, using quantum channels that act directly on the qubits to capture decoherence and operational errors. Specifically, noise is modeled using a depolarizing quantum channel, with two different cases of depolarizing probabilities, 0.03 and 0.2 [41]. The depolarizing channel provides an effective description of decoherence and operational imperfections acting directly on the qubit state. The lower noise level, 0.03, is chosen to enable a direct and fair comparison with the gate-level noise strength employed in the Qiskit simulations. The higher noise level, 0.2, is introduced to probe the robustness of the protocol under stronger decoherence and to examine how the fidelity degrades as noise increases. This allows us to assess the sensitivity of the protocol to noise strength and to gain insight into the range of noise models relevant for more general and large-scale studies. The depolarizing channel is applied after the full encryption-decryption circuit, acting independently on all six qubits (two position qubits and one coin qubit for both Alice and Bob). This approach captures the cumulative effect of noise on the final quantum state, rather than attributing errors to specific gates, and is suited for studying the robustness of the protocol against global qubit decoherence.

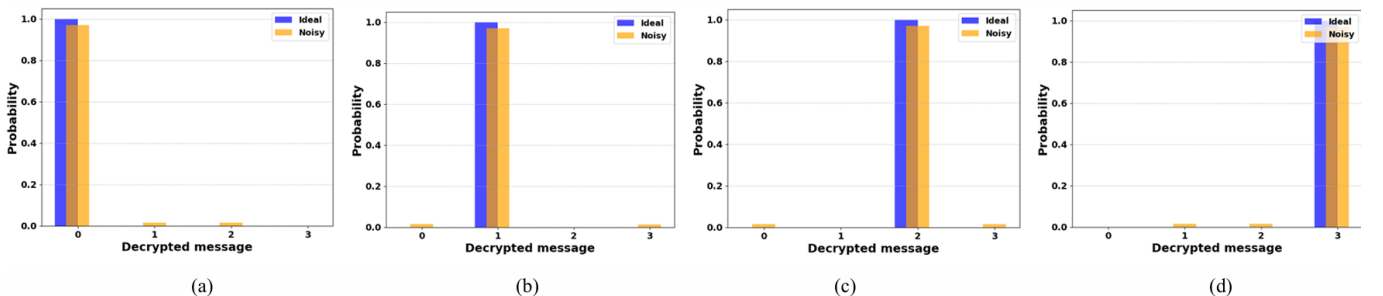


FIG. 13. Probability distribution for the Decrypted message, for encoded message (a)  $k = 0$ , (b)  $k = 1$ , (c)  $k = 2$ , (d)  $k = 3$  with initial position of the walker  $|x\rangle = |0\rangle$  such that the decrypted message is same as the encoded message ( $k' = k$ ) implemented in **Wolfram Quantum Framework** with depolarizing noise (3%) and without noise for  $10^5$  shots on a 4-cycle graph.

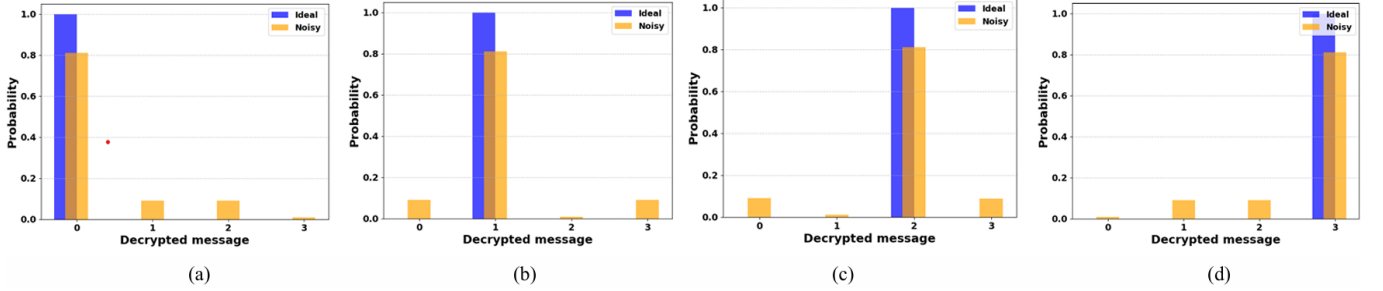


FIG. 14. Probability distribution for the Decrypted message, for encoded message (a)  $k = 0$ , (b)  $k = 1$ , (c)  $k = 2$ , (d)  $k = 3$  with initial position of the walker  $|x\rangle = |0\rangle$  such that the decrypted message is same as the encoded message ( $k' = k$ ) implemented in **Wolfram Quantum Framework** with depolarizing noise (20%) and without noise for  $10^5$  shots on a 4-cycle graph.

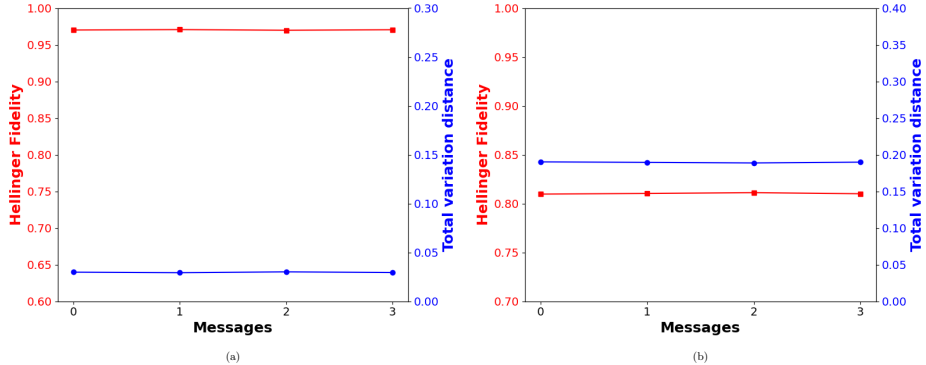


FIG. 15. Hellinger Fidelity and total variance distance for different messages decrypted by Alice with initial position  $|x\rangle = |0\rangle$  and coin  $|l\rangle = |0\rangle$  implemented in **Wolfram Quantum Framework** with (a) less noise (3%) and (b) more noise (20%) for  $10^5$  shots on a 4-cycle graph.

In the absence of noise, the decrypted probability distributions obtained from Mathematica exhibit a sharply peaked structure at the correct message value, reflecting the periodic revival induced by the Parrondo sequence. For each encoded message  $k \in 0, 1, 2, 3$ , the probability of recovering the correct decrypted message  $k' = k$  (for initial state  $|x\rangle = |0\rangle$ ) approaches unity, while the probabilities of the remaining position states are strongly suppressed. This behavior is consistent with the ideal Qiskit simulations and confirms that the Parrondo evolution accurately retraces the public-key dynamics. When depolarizing noise is introduced at the qubit level, the probability distributions broaden, as shown in Figs. 13 and 14 for depolarizing probabilities 0.03 and 0.2. Despite this broadening, the correct decrypted message remains the most probable outcome in all cases. In particular, for the weak noise case, 0.03, the success fidelity of the correct decrypted message is  $\approx 97\%$  (see Fig. 15 (a)), indicating near-ideal recovery despite the presence of realistic qubit-level decoherence. Even for the stronger noise strength, 0.2, the dominant peak corresponding to the correct message persists with fidelity  $\approx 81\%$  (see Fig. 15 (b)), indicating that the periodic revival mechanism survives substantial decoherence. Quantitatively, the noisy Mathematica results show a redistribution of probability mass from the correct message to neighboring position states, while preserving a clear statistical bias toward the correct outcome. This behavior mirrors the trends observed in the Qiskit simulations, where noise reduces fidelity but does not eliminate successful decryption. The agreement between the two platforms confirms that the observed robustness is an intrinsic feature of the Parrondo-driven discrete-time quantum walk dynamics. The comparative performance of the protocol implemented in `qiskit_aer` and the **Wolfram Quantum Framework**, under varying noise strengths, is summarized in Table II.

### Appendix C: NISQ Implementation of the cryptographic protocol: Results and Challenges

Here, we present the results that we obtained via the implementation of the proposed Parrondo's paradox-based cryptographic protocol on a superconducting qubit-based quantum computer, `ibm_torino`, a 133-qubit device under the *Heron r1* processor. The quantum system is accessed via IBM cloud services [36]. This section focuses on the

Methods	Noise type	Noise level	Hellinger Fidelity	Total Variation distance
<code>qiskit_aer</code>	Depolarizing Gate noise	0.03	$\approx 80\%$	$\approx 20\%$
<code>Wolfram Quantum Framework</code>	Depolarizing qubit noise	0.03	$\approx 97\%$	$\approx 3\%$
<code>Wolfram Quantum Framework</code>	Depolarizing qubit noise	0.2	$\approx 81\%$	$\approx 19\%$

TABLE II. Comparison between the results obtained for the proposed cryptographic protocol implemented in `qiskit_aer` and `Wolfram Quantum Framework`

realization of communication between Alice and Bob using different quantum state-transfer strategies, namely direct state transfer via only SWAP operations and hybrid schemes combining SWAP and quantum teleportation. We analyze how these strategies are affected by qubit placement, device connectivity, and transpiler optimization levels, and compare their impact on circuit depth and decrypted-message fidelity. The results illustrate the trade-offs between preserving the logical separation of communicating parties and mitigating hardware-induced errors, providing insight into the feasibility of distributed cryptographic protocols on current NISQ devices.

### 1. Quantum state Transfer with SWAP gates

In principle, the proposed cryptographic protocol requires Alice and Bob to reside on two spatially separated quantum processors. As such distributed quantum execution is not yet supported on current NISQ platforms, we emulated this setting on a single IBM quantum processor by allocating disjoint and widely separated qubit registers (see, Fig. 16 (a)) to represent Alice (position states are encoded in qubits 11, 12 and coin in qubit 18) and Bob (position states are encoded in qubits 91, 95 and coin in qubit 96). The registers were chosen to be as far apart as possible on the device coupling graph to enforce logical separation.

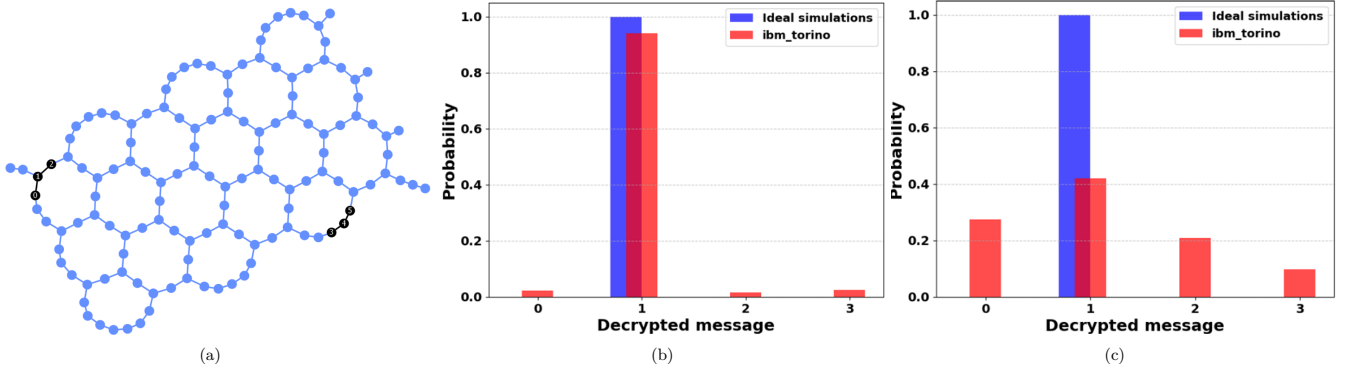


FIG. 16. Realization of the quantum circuit shown in Fig. 11 on the `ibm_torino` processor for  $10^5$  shots on a 4-cycle graph. (a) Qubit layout showing the mapping of Alice's logical qubits (0,1,2) to physical qubits (11,12,18) and Bob's logical qubits (3,4,5) to (91,95,96). (b) Probability distribution of the decrypted message  $k = 1$  obtained by Alice for the initial state  $|x\rangle = |0\rangle$  and  $|l\rangle = |0\rangle$  at transpiler optimization level 3. (c) Corresponding distribution at optimization level 1.

Quantum state transfer between Alice and Bob was implemented through a sequence of SWAP operations across intermediate qubits (see, Algorithm 1 (Fig. 2) in Main). At transpiler optimization level 3 (Fig. 16 (b)), aggressive qubit remapping and gate reordering substantially alter the intended circuit structure, effectively reducing the distinguishability between the Alice and Bob modules. Although this optimization reduces nominal circuit depth, it compromises the logical separation required by the protocol and leads to deviations from the expected behavior. The qubits were initially mapped to separate modules (see, Fig. 16 (a)), but the transpiler optimization compromises the intended communication structure. In particular, only three qubits corresponding to Alice are ultimately retained by the quantum processor, effectively erasing the logical separation between Alice and Bob and rendering any cryptographic message transfer futile. In contrast, optimization level 1 (Fig. 16 (c)) better preserves the logical layout and communication pathways between Alice and Bob, but at the cost of increased circuit depth and a correspondingly decreased fidelity due to higher susceptibility to noise. Fig. 16 thus highlights a fundamental trade-off between structural fidelity and noise resilience on current NISQ hardware. A key limitation of this approach is that it compromises the modular structure required by the cryptographic protocol. To address this, we avoid direct qubit state transfer

and instead explore communication strategies that preserve the logical modules while enabling information transfer, as discussed in the following subsection.

## 2. Quantum State Transfer via SWAP and quantum teleportation operations

To partially mitigate the issue (no effective distinction between the communicating parties) incurred in the previous section, we explored a modified communication strategy in which one stage of state transfer is employed via SWAP operations and the other with quantum teleportation between Alice and Bob. Conceptually, this hybrid approach is closer to a distributed protocol, as teleportation avoids long chains of SWAP operations and reduces qubit state transfer across the device. To implement the hybrid communication protocol, we modify Algorithm 1 (Fig. 2) and present two variants: (i) quantum state transfer via SWAP operations followed by quantum teleportation, and (ii) quantum teleportation followed by a SWAP-based transfer. For both cases, we provide the corresponding Algorithms 3 (Fig. 19) and 4 (Fig. 20) and explicit Qiskit circuit realizations (Figs. 17 and 18) to analyze the impact of operation ordering on preservation of logical modularity. We extend the circuit by three ancilla qubits that are used to generate entangled Bell pairs, allowing the quantum states to be teleported, thereby mimicking inter-module quantum communication. We now proceed to discuss the implementation of this hybrid protocol on `ibm_torino` using different qubit layouts and connectivity between the modules.

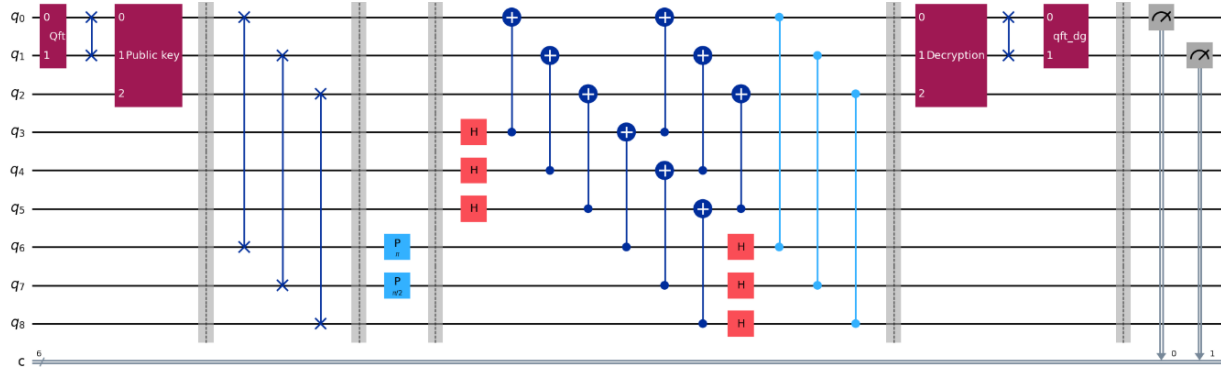


FIG. 17. Quantum circuit implementing the proposed Parrondo's paradox-based cryptographic protocol with hybrid state transfer via SWAP followed by quantum teleportation. Qubits  $q_0, q_1$  and  $q_2$  represent Alice's position and coin degrees of freedom. The public key generated by Alice with initial state  $|000\rangle$  is first transferred to Bob via SWAP operations. Ancilla qubits  $q_3, q_4$  and  $q_5$  generate entanglement between Alice's and Bob's modules for the teleportation stage, while qubits  $q_6, q_7$  and  $q_8$  constitute Bob's module. Bob encodes the message  $k = 1$  on his module, after which the encrypted state is transmitted back to Alice via quantum teleportation, followed by subsequent decryption by Alice.

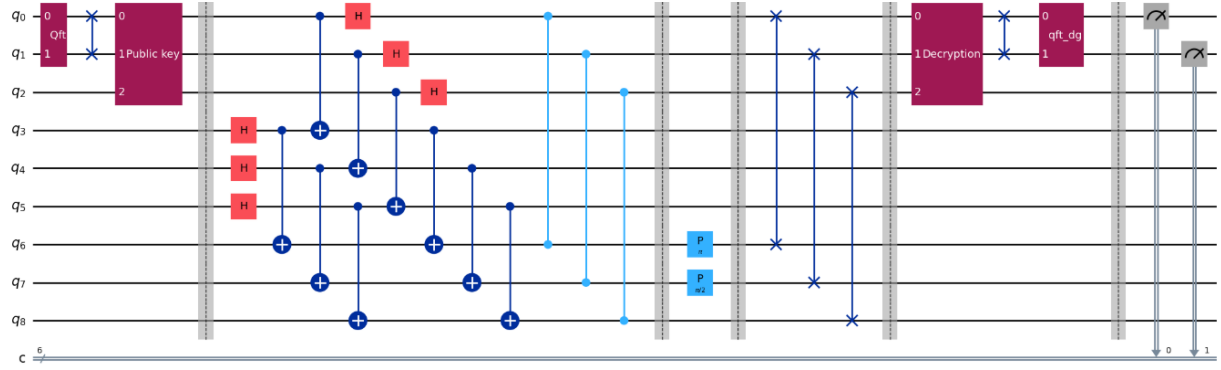


FIG. 18. Quantum circuit implementing the proposed Parrondo's paradox-based cryptographic protocol with hybrid state transfer via quantum teleportation followed by SWAP. Qubits  $q_0, q_1$  and  $q_2$  represent Alice's position and coin degrees of freedom. The public key generated by Alice with initial state  $|000\rangle$  is first transferred to Bob via quantum teleportation. Ancilla qubits  $q_3, q_4$  and  $q_5$  generate entanglement between Alice's and Bob's modules for the teleportation stage, while qubits  $q_6, q_7$  and  $q_8$  constitute Bob's module. Bob encodes the message  $k = 1$  on his module, after which the encrypted state is transmitted back to Alice via SWAP operations followed by subsequent decryption by Alice.

FIG. 19. **Algorithm 3:** Parrondo's Paradox DTQW-based Cryptographic Protocol with state transfer first via SWAP then Teleport (see, Fig. 17)

```

1: Input: Coin operators  $A, B$  generating chaotic DTQW dynamics
2: Design the circuit with 9 qubits: Alice 3 qubits  $q_0q_1q_2$ , Bob 6 qubits: 3 qubits  $q_3q_4q_5$  to generate entanglement, 3
   system qubits  $q_6q_7q_8$ ; Position qubits:  $q_0q_1, q_6q_7$ , Coin qubits:  $q_2$  and  $q_8$ 
   Public Key Generation by Alice
3: Initialize  $q_0q_1q_2$ 
4: Apply QFT on position qubits of Alice  $q_1q_0$ 
5: Apply SWAP on  $q_1q_0$  to get the correct output
6: for  $i = 0$  to  $2$  do
7:   Perform the coin operation  $B$  on  $q_2$ 
8:   Perform the phase rotation  $P(-\pi)$  on  $q_0$ 
9:   Perform the phase rotation  $P(-\pi/2)$  on  $q_1$ 
10:  if  $|q_2\rangle$  is in  $|1\rangle$  then
11:    Perform the phase rotation  $P(\pi)$  on  $q_1$ 
12:  end if
13: end for
   Public Key transfer from Alice to Bob via SWAP
14: Apply the SWAP gates to swap Alice's qubits with Bob's
   Message Encryption by Bob
15: Encrypt the message via  $T_k^D$  operator on Bob's position qubits  $q_6q_7$ 
   Message transfer from Bob to Alice via quantum teleportation
16: Generate Bell pairs  $\frac{|00\rangle+|11\rangle}{\sqrt{2}}$  with qubits  $q_3q_0, q_4q_1, q_5q_2$ 
17: Apply CNOT on qubits  $q_3, q_4, q_5$  with controls  $q_6, q_7, q_8$  respectively.
18: Apply Hadamard gates on qubits  $q_6, q_7, q_8$ .
19: Apply CNOT on qubits  $q_0, q_1, q_2$  with  $q_3, q_4, q_5$  as controls.
20: Apply CZ gates on qubits  $q_0, q_1, q_2$  with  $q_6, q_7, q_8$  as controls.
   Message decryption by Alice
21: for  $i = 0$  to  $18$  do
22:   if  $i \bmod 4 = 0$  or  $i \bmod 4 = 1$  then
23:     Perform the coin operation  $A$  on  $q_2$ 
24:   else
25:     Perform the coin operation  $B$  on  $q_2$ 
26:   end if
27:   Perform the phase rotation  $P(-\pi)$  on  $q_0$ 
28:   Perform the phase rotation  $P(-\pi/2)$  on  $q_1$ 
29:   if  $|q_2\rangle$  is in  $|1\rangle$  then
30:     Perform the phase rotation  $P(\pi)$  on  $q_1$ 
31:   end if
32: end for
33: Apply SWAP on  $q_1q_0$  to get the correct output
34: Apply IQFT on position qubits  $q_1q_0$ 
35: Alice measures her position qubits  $q_1q_0$ 

```

FIG. 20. **Algorithm 4:** Parrondo's Paradox DTQW-based Cryptographic Protocol with state transfer first via teleport then SWAP(see, Fig. 18)

```

1: Input: Coin operators  $A, B$  generating chaotic DTQW dynamics
2: Design the circuit with 9 qubits: Alice 6 qubits: 3 system qubits  $q_0q_1q_2$ , 3 qubits  $q_3q_4q_5$  to generate entanglement,
   Bob 3 qubits  $q_6q_7q_8$ ; Position qubits:  $q_0q_1, q_6q_7$ , Coin qubits:  $q_2$  and  $q_8$ 
   Public Key Generation by Alice
3: Initialize  $q_0q_1q_2$ 
4: Apply QFT on position qubits of Alice  $q_1q_0$ 
5: Apply SWAP on  $q_1q_0$  to get the correct output
6: for  $i = 0$  to  $2$  do
7:   Perform the coin operation  $B$  on  $q_2$ 
8:   Perform the phase rotation  $P(-\pi)$  on  $q_0$ 
9:   Perform the phase rotation  $P(-\pi/2)$  on  $q_1$ 
10:  if  $|q_2\rangle$  is in  $|1\rangle$  then
11:    Perform the phase rotation  $P(\pi)$  on  $q_1$ 
12:  end if
13: end for
   Public Key transfer from Alice to Bob via quantum teleportation
14: Generate Bell pairs  $\frac{|00\rangle+|11\rangle}{\sqrt{2}}$  with qubits  $q_3q_6, q_4q_7, q_5q_8$ 
15: Apply CNOT on qubits  $q_3, q_4, q_5$  with controls  $q_0, q_1, q_2$  respectively.
16: Apply Hadamard gates on qubits  $q_0, q_1, q_2$ .
17: Apply CNOT on qubits  $q_6, q_7, q_8$  with  $q_3, q_4, q_5$  as controls.
18: Apply CZ gates on qubits  $q_6, q_7, q_8$  with  $q_0, q_1, q_2$  as controls.
   Message Encryption by Bob
19: Encrypt the message via  $T_k^D$  operator on Bob's position qubits  $q_6q_7$ 
   Message transfer from Bob to Alice via SWAP
20: Apply the SWAP gates to swap Bob's qubits with Alice's
   Message decryption by Alice
21: for  $i = 0$  to  $18$  do
22:   if  $i \bmod 4 = 0$  or  $i \bmod 4 = 1$  then
23:     Perform the coin operation  $A$  on  $q_2$ 
24:   else
25:     Perform the coin operation  $B$  on  $q_2$ 
26:   end if
27:   Perform the phase rotation  $P(-\pi)$  on  $q_0$ 
28:   Perform the phase rotation  $P(-\pi/2)$  on  $q_1$ 
29:   if  $|q_2\rangle$  is in  $|1\rangle$  then
30:     Perform the phase rotation  $P(\pi)$  on  $q_1$ 
31:   end if
32: end for
33: Apply SWAP on  $q_1q_0$  to get the correct output
34: Apply IQFT on position qubits  $q_1q_0$ 
35: Alice measures her position qubits  $q_1q_0$ 

```

*a. Layout 1: Alice and Bob widely separated*

For this case, we retain the same modular layout shown in Fig. 16 (a) and introduce additional qubits to generate Bell pairs required for the teleportation stage of the hybrid protocol. The qubit layout is depicted in Fig 21 (a). The circuits shown in Figs. 17 and 18 are realized in `ibm_torino` at optimization level 3 with qubits  $q_0q_1q_2$  encoded in physical qubits 11, 12, 18,  $q_3q_4q_5$  in 31, 30, 29 and  $q_6q_7q_8$  in 91, 95, 96.

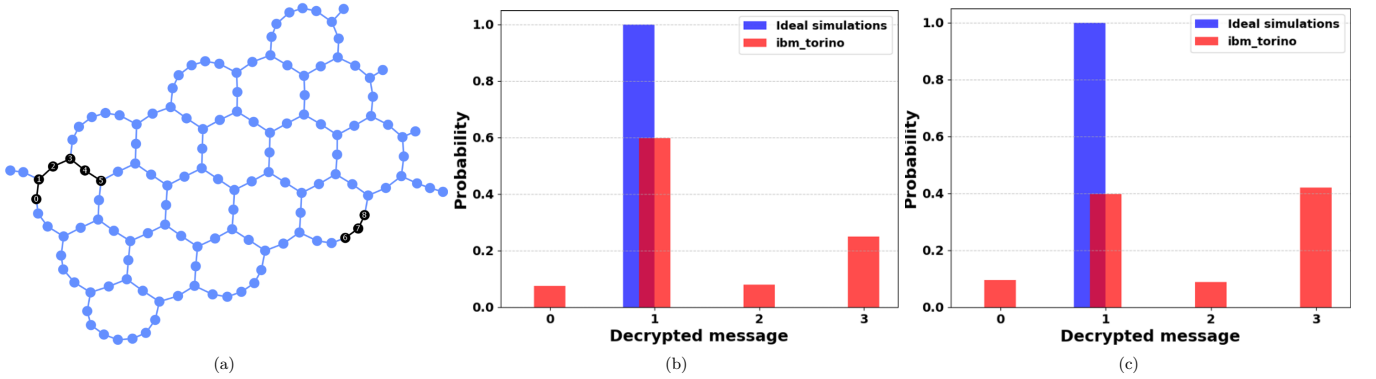


FIG. 21. Hybrid state-transfer implementation of the Qiskit circuits on the `ibm_torino` processor for  $10^5$  shots at transpiler optimization level 3. (a) Qubit layout with Alice’s module on logical qubits (0,1,2), entanglement-generation ancilla qubits on (3,4,5), and Bob’s module on (6,7,8). Probability distribution of the decrypted message  $k = 1$  obtained using the state transfer scheme with (b) first teleportation, then SWAP (Fig. 18 as the Qiskit circuit), and (c) first SWAP then teleport (Fig. 17 as the Qiskit circuit). Logical modules are mapped to physical qubits (11,12,18) for Alice, (91,95,96) for Bob, and (31,30,29) for the ancilla qubits.

Figs. 21 (b) and (c) show the probability distribution of the decrypted message for  $k = 1$  obtained using the hybrid state-transfer protocol. When the circuits are realized in `qiskit_aer` under ideal (noise-free) conditions, the decrypted message is recovered successfully with unit probability for both schemes, confirming the correctness of the circuit construction. When implemented on the NISQ hardware, although the correct decrypted message is still recovered as the most probable outcome, the fidelity is reduced ( $\approx 59.6\%$  for (b) and  $\approx 39\%$  for (c)), indicating partial degradation of the protocol due to the increase in system size together with hardware noise and gate imperfections. Importantly, the hybrid communication strategy preserves the intended communication structure, namely the logical distinction between Alice and Bob, which is otherwise compromised in purely SWAP-based implementations. A comparison of panels (b) and (c) further reveals that the ordering of the communication primitives affects the observed fidelity, with differences arising from how errors accumulate during SWAP operations and teleportation. Motivated by these observations, we examine alternative qubit layouts in the following section to assess whether performing SWAP followed by teleportation is more favorable than teleportation followed by SWAP on current-generation quantum hardware, where qubits and the two-qubit gates remain imperfect.

#### b. Layout 2: Alice and Bob moderately separated

In this section, we consider two distinct reduced-separation configurations, shown in Figs. 22 (a) and 23 (a). Although both layouts reduce the logical distance between Alice and Bob, they differ in the specific physical qubits and connectivity patterns on the hardware, leading to contrasting performance trends. Fig. 22 (a) shows the qubit layout, where Alice and Bob are placed closer on the `ibm_torino` coupling graph while still maintaining distinct logical modules with qubits  $q_0q_1q_2$  encoded in physical qubits 3, 4, 5,  $q_3q_4q_5$  in 16, 23, 24, and  $q_6q_7q_8$  in 37, 52, 51.

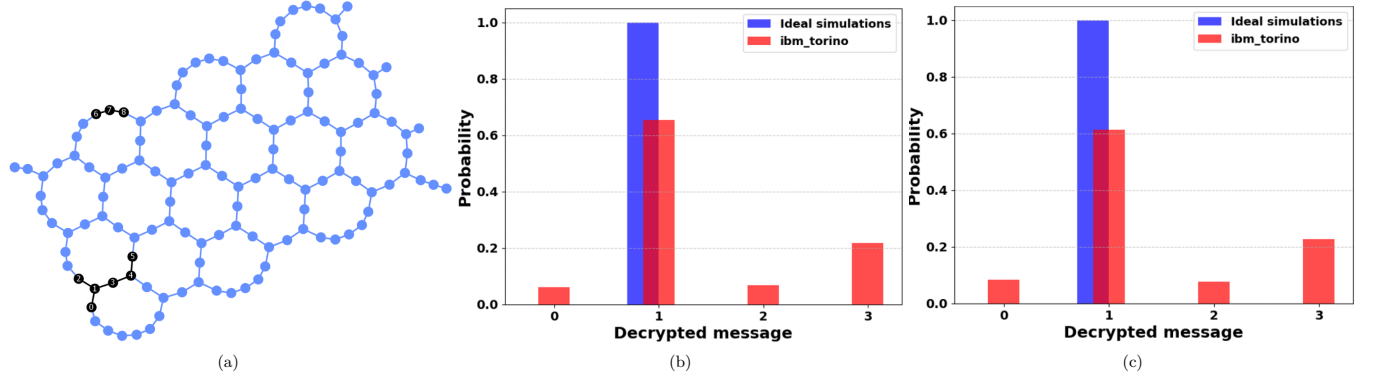


FIG. 22. Hybrid state-transfer implementation of the Qiskit circuits on the `ibm_torino` processor for  $10^5$  shots at transpiler optimization level 3. (a) Qubit layout with Alice’s module on logical qubits (0,1,2), entanglement-generation ancilla qubits on (3,4,5), and Bob’s module on (6,7,8). Probability distribution of the decrypted message  $k = 1$  obtained using the state transfer scheme with (b) first teleportation, then SWAP (Fig. 18 as the Qiskit circuit), and (c) first SWAP then teleport (Fig. 17 as the Qiskit circuit). Logical modules are mapped to physical qubits (3,4,5) for Alice, (37,52,51) for Bob, and (16,23,24) for the ancilla qubits.

Figs. 22 (b) and (c) present the probability distributions of the decrypted message for  $k = 1$  obtained using the hybrid state-transfer protocol with the layout depicted in Fig. 22 (a). While ideal simulations yield unit-probability recovery of the correct message, execution on IBM hardware results in a broadened distribution. A direct comparison of panels (b) and (c) shows that the SWAP-then-teleport strategy yields lower fidelity ( $\approx 61.3\%$ ) than the teleport-then-SWAP strategy ( $\approx 65.3\%$ ), underscoring how errors associated with Bell-pair generation, measurements, and additional two-qubit gates accumulate in the circuit. To examine whether the SWAP-then-teleport ordering can yield improved performance under a different qubit configuration, we next consider an alternative layout, given in Fig. 23 that modifies the choice of physical qubits and their connectivity on the device coupling graph.

Fig. 23 (a) shows the qubit layout, where Alice and Bob are placed closer on the `ibm_torino` coupling graph while still maintaining distinct logical modules with qubits  $q_0q_1q_2$  encoded in physical qubits 3, 4, 5,  $q_3q_4q_5$  in 11, 12, 18, and  $q_6q_7q_8$  in 31, 30, 29.

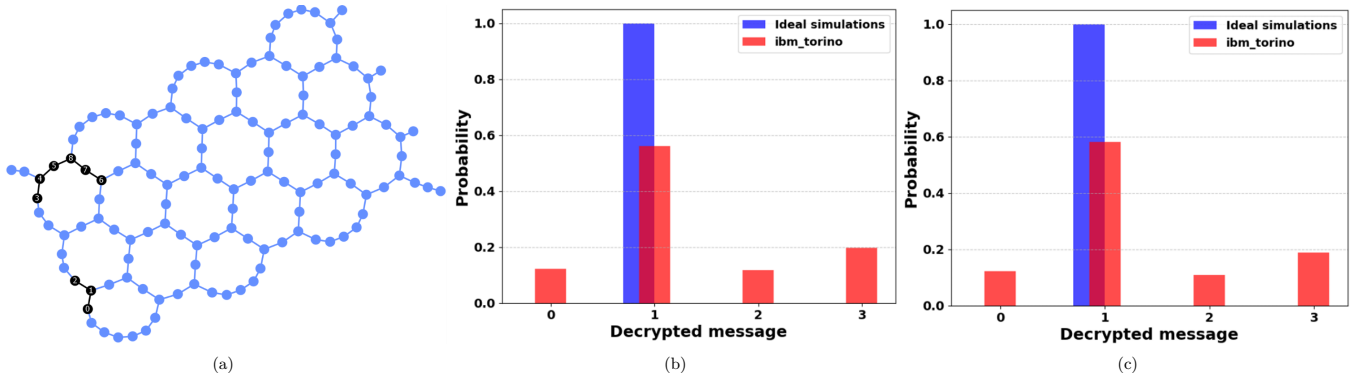


FIG. 23. Hybrid state-transfer implementation of the Qiskit circuits on the `ibm_torino` processor for  $10^5$  shots at transpiler optimization level 3. (a) Qubit layout with Alice’s module on logical qubits (0,1,2), entanglement-generation ancilla qubits on (3,4,5), and Bob’s module on (6,7,8). Probability distribution of the decrypted message  $k = 1$  obtained using the state transfer scheme with (b) first teleportation, then SWAP (Fig. 18 as the Qiskit circuit), and (c) first SWAP then teleport (Fig. 17 as the Qiskit circuit). Logical modules are mapped to physical qubits (3,4,5) for Alice, (31,30,29) for Bob, and (11,12,18) for the ancilla qubits.

Figs. 23 (b) and (c) show the probability distributions of the decrypted message for  $k = 1$  obtained using the hybrid state-transfer scheme implemented on `ibm_torino` with the layout depicted in Fig. 23 (a). A direct comparison of panels (b) and (c) reveals that the SWAP-then-teleport (fidelity  $\approx 58\%$ ) strategy yields higher fidelity than the

teleport-then-SWAP (fidelity  $\approx 56\%$ ) strategy, for this specific choice of physical qubits, indicating that the relative ordering of communication primitives remains strongly conditioned on the underlying qubit layout and connectivity. However, the overall fidelity in this layout (see, Fig. 23 (a)) is reduced in comparison to the previous reduced-separation configuration (see, Fig. 22 (a)). These results further highlight the strong dependence of protocol performance on choice of physical qubits, and demonstrate that the optimal ordering of SWAP and teleportation operations is inherently hardware dependent.

Motivated by the strong dependence of performance on qubit choice and connectivity, we next consider a qubit layout that exploits a fully connected architecture, allowing us to minimize routing overhead and further isolate the impact of hardware noise from connectivity-induced errors.

### c. Layout 3: Fully connected modules

Figs. 24 (a) shows the qubit layout, where Alice and Bob are fully connected on the `ibm_torino` coupling graph with qubits  $q_0q_1q_2$  encoded in physical qubits 28, 29, 30,  $q_3q_4q_5$  in 31, 36, 47, and  $q_6q_7q_8$  in 48, 49, 50. Fig. 24 (b) and (c)

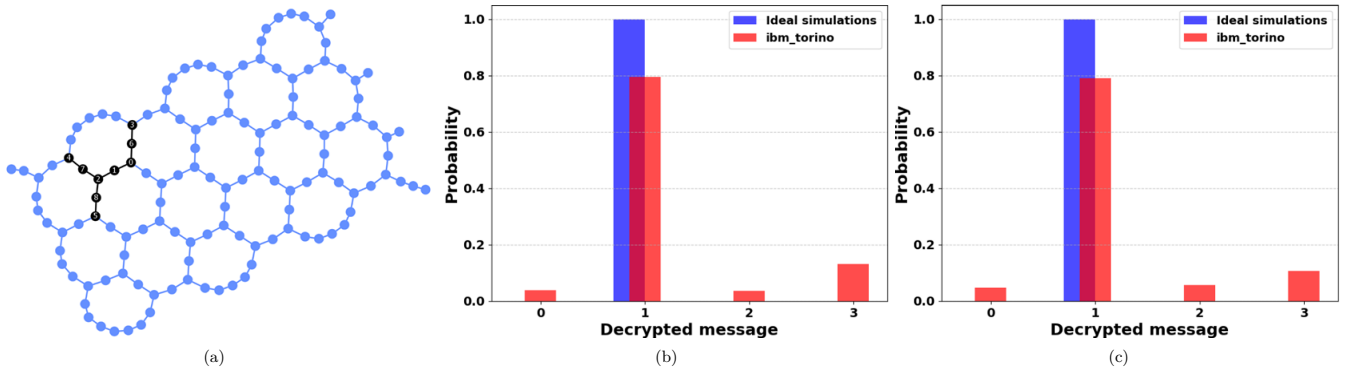


FIG. 24. Hybrid state-transfer implementation of the Qiskit circuits on the `ibm_torino` processor for  $10^5$  shots at transpiler optimization level 3. (a) Fully connected qubit layout with Alice’s module on logical qubits (0,1,2), entanglement-generation ancilla qubits on (3,4,5), and Bob’s module on (6,7,8). Probability distribution of the decrypted message  $k = 1$  obtained using the state transfer scheme with (b) first teleportation, then SWAP (Fig. 18 as the Qiskit circuit), and (c) first SWAP then teleport (Fig. 17 as the Qiskit circuit). Logical modules are mapped to physical qubits (28,29,30) for Alice, (48,49,50) for Bob, and (31,36,47) for the ancilla qubits.

show the probability distribution of the decrypted message for  $k = 1$  obtained using the hybrid state-transfer protocol when Alice and Bob are embedded within a fully connected register architecture on the `ibm_torino` processor. In the ideal simulations, the decrypted message is recovered with unit probability for both hybrid variants. On hardware, the fully connected layout leads to a marked improvement in fidelity compared to the previous layouts, as reduced routing overhead and improved connectivity suppress error accumulation from long SWAP chains. Although hardware noise and gate imperfections still broaden the output distribution, the correct decrypted message exhibits a significantly higher fidelity ( $\approx 79\%$ ) in both panels. Overall, these results demonstrate that access to highly connected qubit modules plays a crucial role in preserving fidelity on current-generation quantum hardware.

Taken together, these results demonstrate that the principal obstacle is not the cryptographic protocol itself, but the lack of true hardware-level modularity and inter-processor connectivity in current NISQ platforms. When implemented on a single quantum processor, the protocol either collapses into an effectively single-module computation due to transpiler optimizations or suffers severe fidelity loss due to excessive circuit depth and noise when modularity is enforced manually. The results of the NISQ implementation of the proposed cryptographic protocol, comparing different state-transfer strategies and qubit layouts used for the Alice and Bob modules, are summarized in Table III. It highlights how the choice of communication method, circuit depth (number of sequential operations of gate layers), and module connectivity jointly influence decryption fidelity.

Together, these observations underscore the present limitations of faithfully realizing spatially separated cryptographic protocols on a single quantum processor. They motivate our simulation-based, proof-of-principle validation, while illustrating the practical challenges that must be addressed before such protocols can be reliably deployed on current NISQ hardware.

State transfer Protocol (Opt.level)	Qubits required	Transpiled qubits	Distinction between Modules	Module	Physical Qubit Layout	Depth	Hellinger Fidelity	Remarks
only SWAPs (3)	6	3	Lost	Widely Separated	11,12,18, 91,95,96	36	94%	Implementation invalid
only SWAPs (1)	6	45	Preserved	Widely Separated	11,12,18, 91,95,96	350	41%	Fidelity below threshold
Teleport then SWAP (3)	9	45	Preserved	Widely Separated	11,12,18, 31,30,29, 91,95,96	188	$\approx 59\%$	Acceptable
SWAP then Teleport (3)	9	45	Preserved	Widely Separated	11,12,18, 31,30,29, 91,95,96	204	$\approx 39\%$	Fidelity below threshold
Teleport then SWAP (3)	9	24	Preserved	Moderately Separated	26,27,28, 29,36,48, 60,59,72	193	$\approx 29.4\%$	Fidelity below threshold
SWAP then Teleport (3)	9	24	Preserved	Moderately Separated	26,27,28, 29,36,48, 60,59,72	198	$\approx 32.9\%$	Fidelity below threshold
SWAP then Teleport (3)	9	17	Preserved	Moderately Separated	3,4,5, 11,12,18, 31,30,29	139	$\approx 58\%$	Acceptable
Teleport then SWAP (3)	9	17	Preserved	Moderately Separated	3,4,5, 11,12,18, 31,30,29	160	$\approx 56\%$	Acceptable
Teleport then SWAP (3)	9	17	Preserved	Moderately Separated	31,30,29, 11,12,18, 3,4,5	137	$\approx 67\%$	Improved performance
SWAP then teleport (3)	9	26	Preserved	Moderately Separated	3,4,5, 16,23,24, 37,52,51	161	$\approx 61.3\%$	Improved performance
Teleport then SWAP (3)	9	26	Preserved	Moderately Separated	3,4,5, 16,23,24, 37,52,51	169	$\approx 65.342\%$	Improved performance
SWAP then Teleport (3)	9	26	Preserved	Moderately Separated	37,52,51, 3,4,5, 16,23,24	184	$\approx 61.9\%$	Improved performance
Teleport then SWAP (3)	9	9	Preserved	Fully Connected	28,29,30, 31,36,47, 48,49,50	100	$\approx 79\%$	Optimal
SWAP then Teleport (3)	9	9	Preserved	Fully Connected	28,29,30, 31,36,47, 48,49,50	98	$\approx 79\%$	Optimal

TABLE III. Comparison of the proposed cryptographic protocol implemented on `ibm_torino` using different state-transfer methods. Note: The first SWAP-only protocol (optimization level 3) is not a valid implementation, as the distinction between Alice and Bob is lost. Rest all approaches remain valid, with differing fidelities.

---

[1] C. Bennett and G. Brassard, Quantum cryptography: Public key distribution and coin tossing, Proc. IEEE Int. Conf. on Computers, Systems and Signal Processing, 175, 8 (1984).

[2] A. Ekert, Quantum cryptography based on Bell's theorem Phys. Rev. Lett., 67, 661 (1991).

[3] W. Wootters, W. Zurek, A single quantum cannot be cloned. Nature 299, 802 (1982).

[4] H. Lo, X. Ma, and K. Chen, Decoy State Quantum Key Distribution, Phys. Rev. Lett. 94, 230504 (2005).

[5] H. Lo, M. Curty, and B. Qi, Measurement-Device-Independent Quantum Key Distribution, Phys. Rev. Lett. 108, 130503 (2012).

[6] U. Vazirani and T. Vidick, Fully Device-Independent Quantum Key Distribution, Phys. Rev. Lett. 113, 140501 (2014).

[7] Y. Zhao, B. Qi, X. F. Ma, H.-K. Lo, and L. Qian, Experimental quantum key distribution with decoy states, Phys. Rev. Lett. 96(7), 070502 (2006).

[8] C. H. Bennett, Experimental quantum cryptography, J. Cryptology 5(1), 3 (1992).

[9] Z. Tang, Z. F. Liao, F. H. Xu, B. Qi, L. Qian, and H.-K. Lo, Experimental demonstration of polarization encoding measurement-device-independent quantum key distribution, Phys. Rev. Lett. 113, 140501 (2014).

tion, Phys. Rev. Lett. 112(19), 190503 (2014).

[10] K. Bharti, et. al., Noisy intermediate-scale quantum algorithms, Rev. Mod. Phys. 94, 015004 (2022).

[11] Y. Aharonov, L. Davidovich, and N. Zagury, Quantum random walks, Phys. Rev. A, 48, 1687 (1993).

[12] J. Kempe, “Quantum random walks: An introductory overview”, Contemporary Physics 44, 307 (2003)

[13] T. Loke, J. B. Wang, Efficient quantum circuits for continuous-time quantum walks on composite graphs. J. Phys. A Math. Theor., 50, 055303 (2017).

[14] P. R. Dukes, Quantum state revivals in quantum walks on cycles, Results in Physics, 4, 189 (2014).

[15] J. Parrondo, L. Dinis, Brownian motion and gambling: from ratchets to paradoxical games, Contemp. Phys. 45, 147 (2004).

[16] G. P. Harmer and D. Abbott, Losing strategies can win by Parrondo’s paradox, Nature, 402, 864 (1999).

[17] M. Jan, Q. Wang, X. Xu, W. Pan, Z. Chen, Y. Han, C. Li, G. Guo, and D. Abbott, Experimental realization of Parrondo’s paradox in 1D quantum walks, Adv. Quantum Technol. 3, 1900127 (2020).

[18] G. P. Harmer and D. Abbott, Parrondo’s Paradox, Statistical Science, 14, 2, 206-213 (1999).

[19] A. Panda and C. Benjamin, Order from chaos in quantum walks on cyclic graphs, Phys. Rev. A, 104, 012204 (2021).

[20] A. Rath, D. K. Panda, and C. Benjamin, Controlling quantum chaos via Parrondo strategies on noisy intermediate-scale quantum hardware, Phys. Rev. E 112, 054219 (2025).

[21] D. Panda and C. Benjamin, Quantum cryptographic protocols with dual messaging system via 2D alternate quantum walk of a genuine single-photon entangled state, J. Phys. A: Math. and Theor. 58, 01LT01 (2025).

[22] A. Alanezi, A. Latif, H. Kolivand and B. Atty, Quantum walks-based simple authenticated quantum cryptography protocols for secure wireless sensor networks, New J. Phys. 25 123041 (2023).

[23] Y. Yang, Q. Pan, S. Sun, and P. Xu. Novel image encryption based on quantum walks. Scientific Reports, 5:7784, 01 (2015).

[24] C. Vlachou, W. Krawec, P. Mateus, N. Paunkovic and A. Souto, Quantum key distribution with quantum walks, Quantum Information Processing, 17(11):288 (2018).

[25] C. Vlachou, J. Rodrigues, P. Mateus, N. Paunkovic, A. Souto, Quantum walk public-key cryptographic system, Int. J. Quantum Inf. 13, 1550050 (2015).

[26] D. Panda and C. Benjamin, Recurrent generation of maximally entangled single-particle states via quantum walks on cyclic graphs, Phys. Rev. A 108, L020401 (2023).

[27] L. Razzoli, G. Cenedese, M. Bondani, and G. Benenti, Efficient Implementation of Discrete-Time Quantum Walks on Quantum Computers, Entropy, 26, 313 (2024).

[28] Qiskit Contributors. Qiskit: An Open-source Framework for Quantum Computing. 2023. Available online: <https://www.ibm.com/quantum/qiskit>

[29] V. Gaur, D. Mehrab, A. Aggarwal, R. Kumari, and S. Rawat Quantum key distribution: attacks and solutions Proc. Int. Conf. on Innovative Computing & Communications (2020).

[30] Wolfram Research, Inc., Mathematica, Version 14.3 (2025) <https://www.wolfram.com/mathematica>

[31] J. Preskill, Quantum Computing in the NISQ era and beyond, Quantum 2, 79 (2018).

[32] M. Caleffi, M. Amoretti, D. Ferrari, J. Illiano, A. Manzalini, A. Cacciapuoti, Distributed quantum computing: A survey, Computer Networks, 254, 110672, ISSN 1389-1286 (2024).

[33] M. A. Nielsen, and I. L. Chuang, Quantum Computation and Quantum Information: 10th Anniversary Edition. 10th Edition, Cambridge University Press, New York (2011).

[34] D. Trevisan, Lecture Notes on Mathematical Aspects of Quantum Information Theory. 2023. Available online: <https://people.cs.dm.unipi.it/trevisan/teaching/PhD/2022-qinfo/2022-Qinfo-notes.pdf>

[35] E. Hellinger, Neue Begründung der Theorie quadratischer Formen von unendlich vielen Veränderlichen, Journal für die reine und angewandte Mathematik, 136, 210–271 (1909).

[36] IBM Quantum. Available online: <https://quantum.ibm.com/>

[37] Wolfram Research, Inc. Wolfram Quantum Framework. Wolfram Research, Inc. (2025), <https://www.wolfram.com/quantum-computation-framework/>

[38] N. Gisin, G. Ribordy, W. Tittel, and H. Zbinden, “Quantum cryptography,” Rev. Mod. Phys., 74, 145, (2002).

[39] A. Almanalky, et. al, Deterministic remote entanglement using a chiral quantum interconnect, Nature Physics, 21, 825 (2025).

[40] A. Rath, D. K. Panda, and C. Benjamin, The Python codes used to generate the numerical results and plots in the study are available in the public repository GitHub, see <https://www.github.com/aaddycool/Parrondo-Paradox-based-Cryptographic-protocol/>

[41] M. Bahrami, Introduction to quantum computing, Wolfram Research, Inc., (2025) .